



T.C.
SELÇUK UNIVERSITY
THE GRADUATE SCHOOL OF NATURAL AND APPLIED SCIENCES



**IMAGE DE-NOISING USING 2-D CIRCULAR-
SUPPORT WAVELET TRANSFORM**

ADIL ABDULSATTAR YASEEN AYDIKI

MASTER THESIS

Department of Information Technology Engineering

May-2018
KONYA
All Rights Reserved

TEZ KABUL VE ONAYI

Adil Abdulsattar Yaseen AYDIKI tarafından hazırlanan “Image De-Noising Using 2-D Circular-Support Wavelet Transform” (İki Boyutlu Sirkülasyon Destekli Dalgacık Dönüşümünü Kullanarak İmgelerde Gürültü Temizlemesi) adlı tez çalışması 30/05/2018 tarihinde aşağıdaki jüri tarafından oy birliği / oy çokluğu ile Selçuk Üniversitesi Fen Bilimleri Enstitüsü Bilişim Teknolojileri Mühendisliği Anabilim Dalı’nda YÜKSEK LİSANS TEZİ olarak kabul edilmiştir.

Jüri Üyeleri

Başkan

Prof. Dr. Fatih BAŞÇİFTÇİ

Danışman

Prof. Dr. Fatih BAŞÇİFTÇİ

Üye

Dr. Öğr. Üyesi Ayşe ELDEM

Üye

Dr. Öğr. Üyesi Tahir SAĞ

İmza



Yukarıdaki sonucu onaylarım.

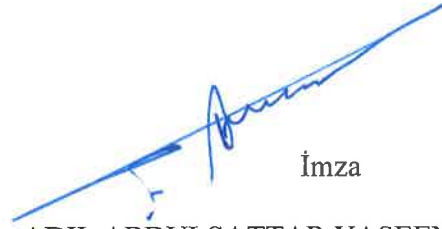
Prof. Dr. Mustafa YILMAZ
FBE Müdürü

TEZ BİLDİRİMİ

Bu tezdeki bütün bilgilerin etik davranış ve akademik kurallar çerçevesinde elde edildiğini ve tez yazım kurallarına uygun olarak hazırlanan bu çalışmada bana ait olmayan her türlü ifade ve bilginin kaynağına eksiksiz atıf yapıldığını bildiririm.

DECLARATION PAGE

I hereby declare that all information in this document has been obtained and presented in accordance with academic rules and ethical conduct. I also declare that, as required by these rules and conduct, I have fully cited and referenced all material and results that are not original to this work.



İmza

ADIL ABDULSATTAR YASEEN AYDIKI

Tarih: 30.05.2018

ABSTRACT

Msc. Thesis

IMAGE DE-NOISING USING 2-D CIRCULAR-SUPPORT WAVELET TRANSFORM

ADIL ABDULSATTAR YASEEN AYDIKI

**THE GRADUATE SCHOOL OF NATURAL AND APPLIED SCIENCE OF
SELCUK UNIVERSITY
THE DEGREE OF MASTER IN INFORMATION TECHNOLOGY
ENGINEERING.**

**Advisor: Prof. Dr. Fatih BAŞÇİFTÇİ
2018, 87 Pages.**

**Jury
Prof. Dr. Fatih BAŞÇİFTÇİ
Asist. Prof. Dr. Ayşe ELDEM
Asist. Prof. Dr. Tahir SAĞ**

A new image de-noising algorithm based on a two-dimensional circular support wavelet transform (2-D CSWT) is proposed. By using the 2-D circular spectral split schemes, in this (2-D CSWT) geometrical image transform, images can be efficiently represented. In such transform, the high-pass and low-pass filters of the 2-D circular-support counterparts can be earned from the traditional 1-D analysis Haar wavelet filter bank branches. Efficient frequency-masking is applied to realize the designed 2-D circular wavelet filter bank branches. In the decomposition stage, a 3-level 2-D circular decomposition with down-sampling by (2, 2) is performed. At each level, low- and high-pass 2-D frequency coefficient channels are obtained on two separable 2-D regions. The input noisy image is decomposed by such 2-D CSWT transform into many 2-D low- and high-pass coefficient channels, depending on the number of the decomposition level. De-noising by thresholding processes can be applied on all 2-D high-pass coefficient channels with different thresholding levels. In the reconstruction stage, a 2-D circular-support reconstruction filter bank with up-sampling by (2, 2) is used to achieve the de-noised image. The performance of such de-noising scheme is evaluated by its examining different noisy images with different noise levels (Salt & Pepper and Gaussian). It is noticed that the proposed circular wavelet scheme can outperform the conventional wavelet de-noising method in terms of correlation factor and Peak Signal to Noise Ratio (PSNR) of the reconstructed images.

Keywords: Back Wavelet, Image Filtering, Wavelet Paket Decomposition, Noise Processing.

ÖZET
YÜKSEK LİSANS TEZİ
İKİ BOYUTLU SİRKÜLASYON DESTEKLİ DALGACIK DÖNÜŞÜMÜNÜ
KULLANARAK İMGELERDE GÜRÜLTÜ TEMİZLEMESİ

ADIL ABDULSATTAR YASEEN AYDIKI

Selçuk Üniversitesi Fen Bilimleri Enstitüsü
Bilişim Teknolojileri Mühendisliği Anabilim Dalı

Danışman: Prof. Dr. Fatih BAŞÇİFTÇİ
2018, 87 Sayfa

Jüri

Prof. Dr. Fatih BAŞÇİFTÇİ
Dr. Öğr. Üyesi Ayşe ELDEM
Dr. Öğr. Üyesi Tahir SAĞ

Yeni bir “İki boyutlu sirkülasyon destekli dalgacık dönüşümüne dayalı ses azaltma algoritması” amaçlanmıştır. (2-D CSWT). 2-D CSWT 2 boyutlu dairesel spektral bölünmüş şemaları etkili bir şekilde sunabilen geometrik bir resim dönüşümüdür (örn. Dairesel olarak parçalanmış frekans alt boşlukları). Böyle bir dönüşümde, klasik tek boyutlu (1-D) haar dalgacıklı düşük geçiş ve yüksek geçiş filtreleri iki boyutlu sirkülasyon destekli eşdeğerlerine dönüşür. Etkili frekans maskeleyesi tasarlanmış olan iki boyutlu dairesel dalgacıklı filtrelerin farkedilmesi için uygulanmıştır. Ayırma evresinde 3 seviyeli alt-örneklemeli bir 2-D sirkülasyon ayrışması (2,2) tarafından gerçekleştirilir. Her seviyede iki boyutlu düşük ve yüksek geçiş frekans katsayı kanalları ayrılabilir iki 2-D bölgesi elde edilir. Ses görselinin girişi 2-D CSWT dönüşümü ile ayrıştırma seviyesine bağlı olarak pek çok iki boyutlu düşük ve yüksek geçiş katsayı kanallarına ayrıştırılır. Eşikleme yaparak ses azaltma işlemi tüm iki boyutlu yüksek geçiş katsayı kanallarında farklı eşikleme seviyeleri ile uygulanabilir. Yeniden kurulum aşamasında sesi azaltılan görseli elde etmek için (2,2) tarafından 2-D sirkülasyon destekli üst örneklemeli yeniden kurulum filtresi kullanılır. Bazı ölçü birimleri kullanılarak, bu tür ses giderme şemalarının performansı farklı gürültülü görüntüler üzerinde test edilerek değerlendirilebilir. Bu ölçü birimleri Ortalama mutlak hata (MAE), Ortalama karesel hata (MSE) ve En yüksek sinyal-gürültü oranı (PSNR) içerebilir.

Anahtar kelimeler: Dalgacık Dönüşümü, Gürültü Temizleme, Dalgacık Paket Ayırıştırması, Görüntü İşleme

ACKNOWLEDGEMENT

All gratitude is to almighty **ALLAH** who guided me and granted me the health, strength, patient and the opportunity to complete my MSc thesis. I would like to thank my Advisor **Prof. Dr. FATİH BAŞÇİFTÇİ** for his supervision, support, and continuous encouragement during the preparation of the thesis.

Also I would like to thank **Prof. Dr. Jasim M. Abdul-Jabbar** for his support for postprocessing my data, and special thanks to **Prof. Dr. Jassim M. Al-Tohma** and **Mr. Omar Yaseen Ismael** for their support and advices.

Special thanks to my friend **Research Assistant Batuhan Eren Engin** for his help at the time of writing my thesis. Special thanks to my family for their incomparable support, motivation and assurance during all my life.

My thanks also to all those who helped me, in one way or another, to achieve my MSc thesis.

ADIL ABDULSATTAR YASEEN AYDIKI
KONYA-2018

TABLE OF CONTENTS

ABSTRACT.....	I
ÖZET	II
ACKNOWLEDGEMENT.....	III
TABLE OF CONTENTS	IV
SYMBOLS AND ABBREVIATIONS	VI
1. INTRODUCTION	2
1.1. Introductory Remarks.....	2
1.2. Aim of the Thesis.....	6
1.3. Thesis Outline	6
2. WAVELET FUNDAMENTALS AND LITERATURE REVIEW	7
2.1. The Wavelet Transform	7
2.2. Conditions of Wavelets.....	10
2.3. Types of Wavelet Transform	11
2.3.1. Continuous wavelet transform	11
2.3.2 Discrete wavelet transform	13
2.4 The Filter Bank	15
2.4.1 Quadrature mirror filter (QMF) banks.....	16
2.4.2. The analysis and the synthesis filter banks.....	16
2.4.3. The perfect reconstruction conditions for QMF banks.....	18
2.5 Filter Bank for Discrete Wavelet Transform	19
2.6. Traditional Structures for Discrete Wavelet Transform	21
2.6.1. Direct form structure.....	21
2.6.2. Poly-phase structure.....	21
2.6.3 Lattice structure	23
2.6.4. Lifting scheme structure	23
2.7. All-Pass Filters.....	24
2.8. FIR and IIR Wavelet Filter Banks	25
2.8.1. Two-channels QMF banks using all-pass filters.....	25
2.8.2 IIR wavelet filter banks.....	27
2.9. Wave Digital Filters (WDFs).....	28
2.9.1. Lattice wave digital filters (LWDFs).....	28
2.9.2. Bi-reciprocal lattice wave digital filters (BLWDFs)	30
2.10. Literature Review	32
3. THE PROPOSED METHODOLOGY AND EFFICIENT REALIZATION	36
3.1. 2-D Circular-Support Wavelet Transform (2-D CSWT).....	36
3.2. 2-D Circular-Support Wavelet Transform for Image De-noising	36
3.3. Efficient and Simplified Structures.....	38
4. TEST RESULTS.....	40

4.1. Results of circular wavelet de-noising by thresholding.....	40
4.1.1. Results of circular wavelet de-noising by thresholding.....	40
4.1.2. Circular wavelet results for images with salt and pepper noise.....	50
4.2. Results of Conventional wavelet de-noising by thresholding	60
4.2.1. Conventional wavelet Results for images with Gaussian noise	60
4.2.2. Conventional wavelet Results for images with salt and pepper Noise	70
4.3. A Comparative Study.....	70
5. CONCLUSIONS AND FUTURE WORK.....	73
5.1. Conclusions.....	73
5.2. Future Works	74
REFERENCES.....	75
ÖZGEÇMİŞ	79



SYMBOLS AND ABBREVIATIONS

Symbols

σ	: Noise deviation
t	: Predicted noise threshold level
$c(n,m)$: Matched coefficient sub-symbol
$g(m,n)$: Noise- clear image
$\Psi(t)$: Mother wavelet
$X(f)$: Signal fourier transform $x(t)$
L	: Lemotes the number of decomdosition levels
$\Psi_{a,0}(t)$: Time- scaled mother wavelet
Ψ_w	: Fourier transform
C	: Admissibility constant
X_{WT}	: Continous wavelet transform
$\psi_{j,k}(t)$: Discrete wavelet transform
$H_p(z)$: Equivalent representation of analysis
$F_p(z)$: Synthesis filter bank
$A(z)$: All-pass filter
$H_0(z)$: Low- pass filter
$H_1(z)$: High-pass filter

Abbreviations

PSNR	: Peak signal noise ratio
MAE	: Mean square error
MSE	: Maximum signal error
STFT	: Short time fourier transform
WT	: Wavelet transform
CWT	: Continuous wavelet transform
QMF	: Quadrature mirror filter
WDF _s	: Wave digital filters
LWDF _s	: Lattice wave digital filters
BLWDF _s	: Bi-reciprocal lattice wave digital filter

1. INTRODUCTION

1.1. Introductory Remarks

Images are often suffering from two main corruptions (unwanted modifications). These modifications in image accuracy are categorized as blur and noise. Blur is intrinsic to image acquisition systems, as digital images have a finite number of samples and must satisfy the Shannon-Nyquist sampling conditions (Buades et al., 2005). The second main image perturbation is noise. Image noise is random variation of brightness or color information in images, and is usually a result of some defects in the handling optical and electronic systems. Noise appears during different image processing phases of acquisition, transmission, and retrieval. The purpose of any de-noising algorithm is to remove such noise while maintaining as much as possible image details (Chen et al., 2006; Shinde et al., 2012). Since some fine details of the image always occupy the same high-pass spectrum, then they will be confused with the noise or vice-versa. The need of an image without noise is a requirement for many image processing algorithms such as pattern recognition, compression, etc. to efficiently work. Such requirements justify the importance of de-noising in images. Images can be affected by different types of noise sources. In a digital camera, noise may be added to the image while passing through lens, sensors, and ADC. In addition, the image processing block itself may add some noise. The types of image noise can range from salt and pepper, additive white Gaussian (AWG) to speckles (Verma and Ali, 2013).

In classical terms, the 1-D wavelet transform of Fig. 1.1 can be extended to 2-D wavelet transform. At each decomposition level, the 1-D transform is first applied across all the rows and then across all the columns to acquire a 2-D transform. At each decomposition level, four coefficients sets are produced: HH as the details across the diagonal direction, HL as the details across the vertical direction, LH as the details across the horizontal direction and LL as the average.

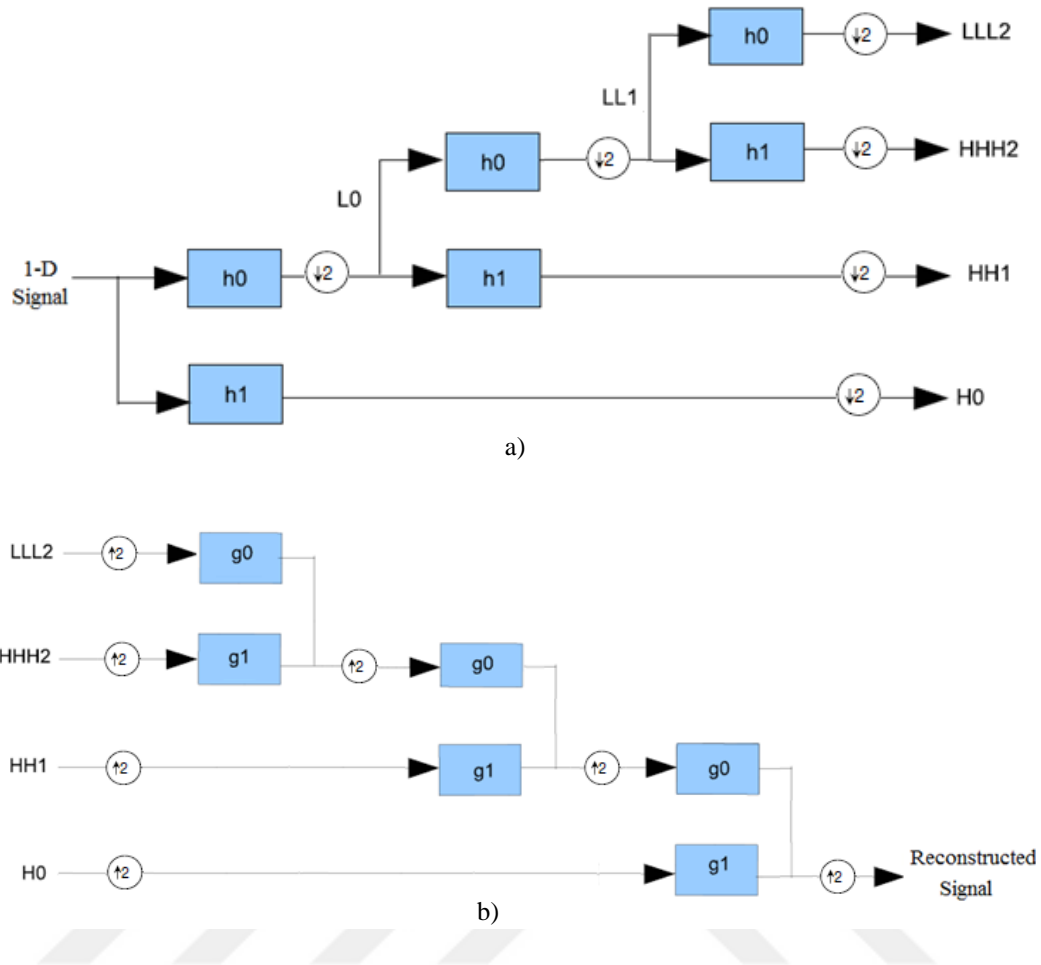


Fig. 1.1 1-D wavelet transform and its inverse. (a) 1-D wavelet 3-level decomposition (wavelet transform WT), (b) 1-D wavelet 3-level reconstruction (inverse wavelet transform IWT).

In 2-D case, the original image signal $x(m, n)$ can be considered as if it is a combination of 1-D row signals and 1-D column signals. As it is done in 1-D case, each row of the image is processed first, in 2-D Discrete Wavelet Transform (DWT), then each column is processed. Figure 1.2 demonstrates a one-level image decomposition and reconstruction. In a similar way as in signal decomposition, the subsampling process is applied after each filtering. The whole process results in four sub-images, namely; approximation component and horizontal, vertical & diagonal details. The resulting sub-images have quarter the size of the original image, that because of the sub-sampling after each filtering.

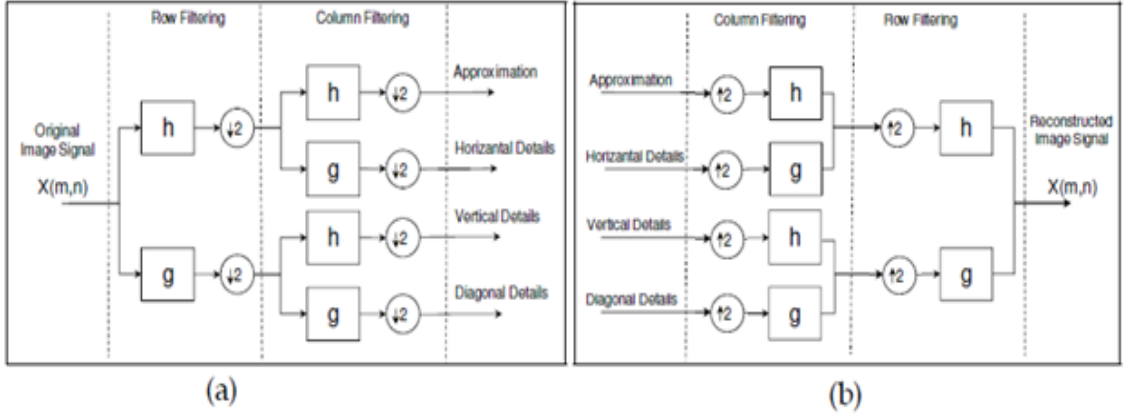


Fig. 1.2. One-level DWT steps of a 2-D image, (a) Decomposition, (b) Reconstruction.

A classical wavelet de-noising scheme is shown in Fig. 1.3, it consists of 2-D wavelet transform, 2-D inverse wavelet transform and an intermediate thresholding stage to shrink wavelet coefficients. In such thresholding stage, the level of the noise is first estimated and the appropriate thresholds are set. It should be noted that setting an appropriate value for the level of thresholding is an important point in thresholding. Recently, to calculate the value of thresholding, many approaches have been given. the estimation of the level of noise is needed by most of those approaches. Though, a useful tool for an estimator is the standard deviation of the data values. A good estimator σ for the wavelet de-noising is proposed by Donoho (Ergen, 2012) and given as;

$$\sigma = \frac{\text{median}(d_{L-1,k})}{0.6745}, \quad k = 0,1, \dots, 2^{L-1} - 1 \quad (1.1)$$

where L denotes the number of decomposition levels. The median selection is applied on the detail coefficient of the decomposed signal.

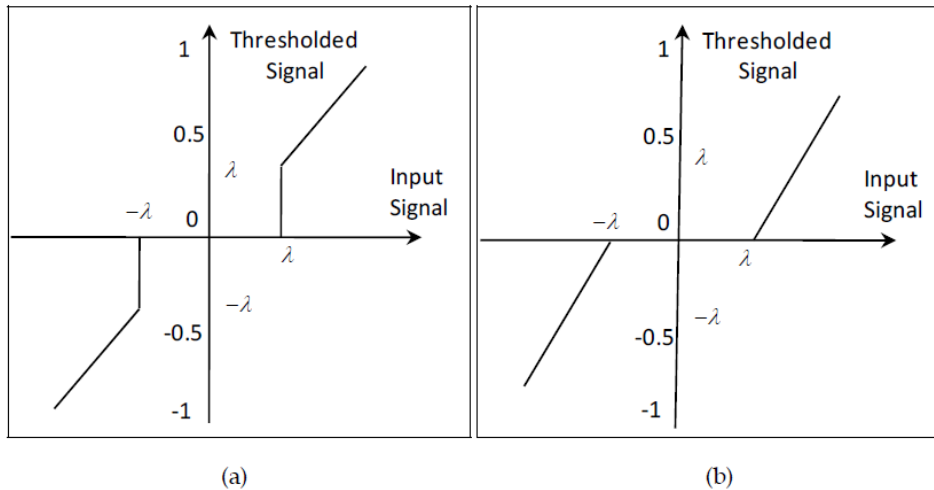


Fig. 1.3. Thresholding strategies, (a) Hard thresholding, (b) Soft thresholding.

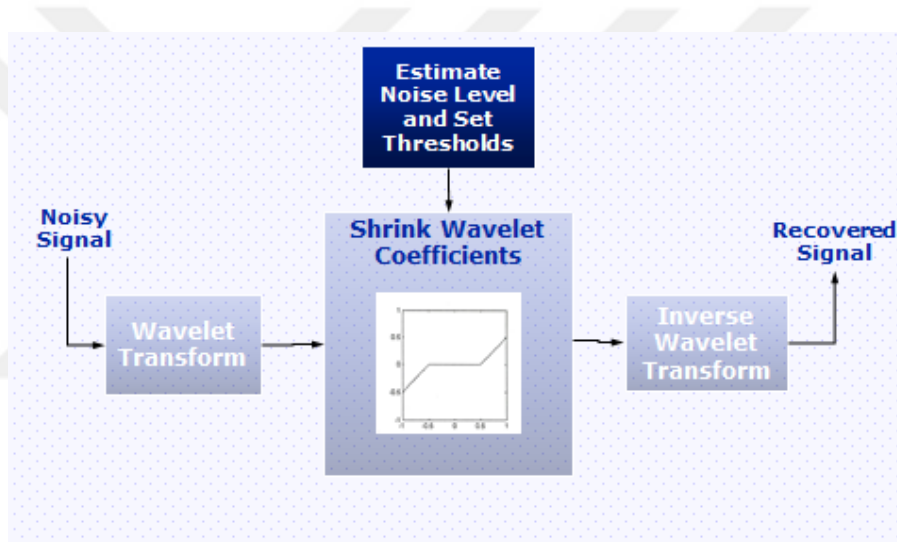


Fig. 1.4. A classical scheme for wavelet de-noising.

In Fig. 1.3, the intermediate stage of wavelet coefficient shrinking (*i. e.*, thresholding) can be performed either by hard thresholding or by soft thresholding strategies (as shown in Fig. 1.4). Generally, thresholding process will allow the detail coefficients which are greater than the threshold level to pass (*i. e.*, considering them as image high frequency components) while preventing the lower level coefficients from passing through the threshold (*i. e.*, considering them as noise components). The two strategies of thresholding are having many limitation and property considerations. Small changes in pixel level can usually very sensitive and unstable to the hard thresholding strategy. On other side, unnecessary level of level for true large coefficients can be occur on the soft thresholding strategy. Many sophisticated methods are proposed to overcome

the drawbacks of the thresholding described nonlinear strategies. Despite that, hard and soft thresholding are still applicable and treated as the most reliable and efficient thresholding techniques.

1.2. Aim of the Thesis

Proposing, constructing and testing a new image de-noising algorithm based on a 2-D CSWT. By using 2-D circular spectral split schemes with the efficient frequency-masking application for the realization of the designed 2-D circular wavelet filter bank branches, this 2-D CSWT is a geometrical image transform can be constructed. Via some metrics, the performance of the proposed system is to be tested. These metrics include correlation factor and Peak signal-to-noise ratio (PSNR) in dB.

1.3. Thesis Outline

In addition to this introduction in Ch.1, four other chapters are included in this thesis. Chapter 2 gives some fundamentals of wavelets and filter banks. Types of wavelet transform are also discussed. In addition, traditional FIR and IIR wavelet filter banks are included. Lattice wave digital filters (LWDFs) are introduced also for IIR filter bank simulation.

In Chapter 3, the proposed methodology is described. The idea of circular wavelet transform is introduced and some properties of such transform are highlighted. A de-noising diagram is proposed using the circular wavelet transform. A 3-decomposition level simplified de-noising structure is also derived with efficient realization.

Chapter 4 contains the implementation and testing of the proposed methodology, showing some results highlighting the performance of the whole de-noising process. In such process, five standard images (including three different levels of two types of noise "Salt & pepper and Gaussian") are tested.

In Chapter 5, conclusions are given with future works.

2. WAVELET FUNDAMENTALS AND LITERATURE REVIEW

Signal transformation is just another form of representing the signal, so that the information content present in the signal will not be changed. The wavelet transform (WT) is a very powerful transform, used in different branches of science. The power of the transform comes from the fact that the basis functions of the transform are localized in time and frequency with their different resolutions.

2.1. The Wavelet Transform

To overcome the shortcoming of the Short Time Fourier Transform (STFT), the wavelet transform was developed and in analyzing the non-stationary signals, it can be used.

Different frequencies are analyzed with different resolutions in the wavelet transform uses multi-resolution technique while the STFT gives a constant resolution at all frequencies. In a multi-carrier system, the wavelet transform can be used as a possible transform to generate sub-channels (Srivastava and Maheshwari, 2015).

As shown in Fig. 2.1, the wave is an oscillating function of time and is periodic, while wavelets are just localized small waves (Mastriani, 2015). The energy of wavelets can be concentrated in time and are suited for analyzing the transient signals. Fourier transform, STFT and wavelet transform are different. The sinusoidal waves to analyze signals are using in the first two types of transformation, while finite energy wavelets are using in the third to transfer the signals (Abdul-Jabbar et al., 2013).

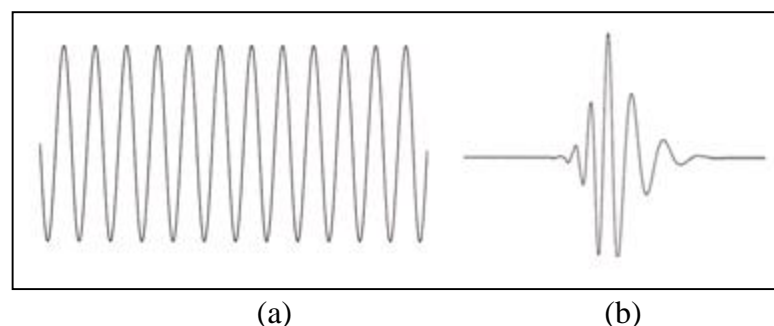


Fig. 2.1 Demonstration of (a) a Wave and (b) a Wavelet, (Srivastava and Maheshwari, 2015).

In the sense that the signal to be analyzed is multiplied with a wavelet function, the STFT analysis is also similar to the wavelet analysis, while it is only multiplied with

a window function in the STFT, and then at each segment generated the transform is computed. Also, in wavelet transform, the wavelet function width changes with each spectral component, while in STFT, the width of the window function is keeping constant. At high frequencies, it gives poor frequency resolution and good time resolution while at low frequencies, the wavelet transform gives poor time resolution and good frequency resolution (Abdul-Jabbar and Abdulkader, 2012; Srivastava and Maheshwari, 2015).

The wavelets are denoted to the functions generated from one single function (basis function) and this single function is called the mother wavelet. Other related wavelets contain dilations (scaling parts) and translations (shift parts) in time domain. The other wavelets $\psi_{a,b}(t)$ can be represented as following while the mother wavelet is denoted by $\psi(t)$:

$$\psi_{a,b}(t) = \frac{1}{\sqrt{|a|}} \psi\left(\frac{t-b}{a}\right) \quad (2.1)$$

where b and a are two random parameters. In the time axis, they denote the parameters for translations and dilations, respectively.

It is obvious from equation (2.1) that the mother wavelet can be essentially represented as

$$\psi(t) = \psi_{1,0}(t) \quad (2.2)$$

For $a \neq 1$ and $b = 0$, $\Psi_{a,0}(t)$ can be written as:

$$\Psi_{a,0}(t) = \frac{1}{\sqrt{|a|}} \psi\left(\frac{t}{a}\right) \quad (2.3)$$

$\psi_{a,0}(t)$ As shown in equation (2.3) is a time-scaled mother wavelet $\psi(t)$ by a factor of a with amplitude-scaling by factor of $1/\sqrt{|a|}$. $a < 1$ stands for time-compression while $a > 1$ reflects time-expansion. That's the reason behind calling the parameter a as dilation (scaling) parameter. When $a < 0$, the function $\psi_{a,b}(t)$ results in reversal of time with dilation [9].

As shown in the resulting wavelet function $\psi_{a,b}(t)$ in eq. (2.1), the mathematically substituting t in eq. (2.3) by $t-b$ will cause a shift or translation in the time axis. The time axis right side will be shifted by a value of b as the function $\psi_{a,b}(t)$ is a shifted version of $\psi_{a,0}(t)$ when $b > 0$ whereas, when $b < 0$, it is a shift in the time axis left side by a value of b . Due to that the variable b will be representing the translation in time domain (shift in phase). In the time domain, the mother wavelet and its dilations will be illustrated as in Fig. 2.2 with the parameter of dilation $a = \alpha$.

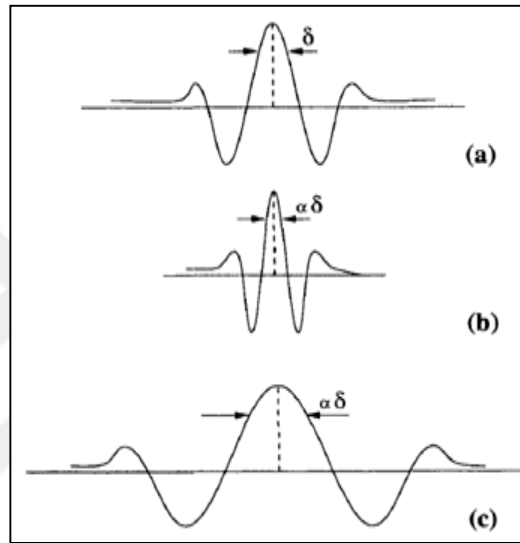


Fig. 2.2. (a) A mother wavelet $\Psi (t)$, (b) $\Psi (t/\alpha) : 0 < \alpha < 1$, (c) $\Psi (t/\alpha) : \alpha > 1$, (Abdul-Jabbar and Abdulkader, 2010).

Fig. 2.2 (a) shows the mother wavelet $\psi(t)$ while a signal with compressed version in the axis of time when $\alpha < 1$ is shown in Fig. 2.2 (b) and Fig. 2.2 (c) is showing the signal expansion in the axis of time when $\alpha > 1$. The wavelet transform of the signal $x(t)$ based on wavelets definition, can mathematically be represented by Abdul-Jabbar and Abdulkader (2010):

$$W(a, b) = \int_{-\infty}^{+\infty} x(t) \psi_{a,b}(t) dt \quad (2.4)$$

Mathematically, the reconstruction of $x(t)$ from $W(a,b)$ inverse transform is represented by:

$$x(t) = \frac{1}{C} \int_{a=-\infty}^{+\infty} \int_{b=-\infty}^{+\infty} \frac{1}{|a|^2} \psi_{a,b}(t) W(a, b) da db \quad (2.5)$$

Where

$$C = \int_{-\infty}^{+\infty} \frac{|\Psi(\omega)|^2}{|\omega|} d\omega \quad (2.6)$$

The Fourier transform of the mother wavelet $\psi(t)$ is $\Psi(\omega)$. $W(a, b)$ in equation (2.4) will be then named continuous wavelet transform (CWT), if $x(t)$ b and a are continuous,. Hence the bi-variant function $W(a, b)$ of two continuous real variables can be gotten from the CWT of a 1-D continuous function $x(t)$, specifically; b as the translation and a as the dilation (Abdul-Jabbar and Abdulkader, 2010).

2.2. Conditions of Wavelets

if the following mathematical criteria are fulfilled, as a wavelet, an analyzing function $\psi(t)$ can be used:

- 1- A finite energy must be in the wavelet *i.e.*,

$$E = \int_{-\infty}^{\infty} |\psi(t)|^2 dt < \infty \quad (2.7)$$

the following condition must hold if $\Psi(\omega)$ is the Fourier transform of the wavelet $\psi(t)$,

$$C = \int_0^{\infty} \frac{|\hat{\psi}(\omega)|^2}{\omega} d\omega < \infty \quad (2.8)$$

C : the admissibility constant.

As per this condition, no zero-frequency component ($\psi(0) = 0$) will be on the wavelet, *i.e.*, the wavelet $\psi(t)$ mean must be equal to zero. Admissibility constant can be named to this condition. The chosen wavelet will be effecting the value of C .

It is well known that wavelets can be classified into two classes: (a) orthogonal and (b) bi-orthogonal. Based on the application, either of them can be used (Shinde et al., 2012).

2.3. Types of Wavelet Transform

2.3.1. Continuous wavelet transform

The continuous wavelet transform (CWT) is normally represented by

$$X_{WT}(\tau, s) = \frac{1}{\sqrt{|s|}} \int x(t) \cdot \psi^* \left(\frac{t - \tau}{s} \right) dt \quad (2.9)$$

with $s=a$ and $\tau=b$. ψ^* : is the conjugate of $\psi(t)$.

where $x(t)$ is the signal to be analyzed. $\psi(t)$ is the mother wavelet or the basis function. A mother wavelet can generate all the wavelet functions that can be utilized in the transformation through translation (shifting) and scaling (dilation or compression) (Abdul-Jabbar and Abdulkader, 2012).

A limitation in STFT is the use of only one window size for all frequencies (see Fig. 2.3 (a)), so the resolution of the analysis in the time-frequency plane is unchanged at all locations as shown in Fig. 2.3 (b).

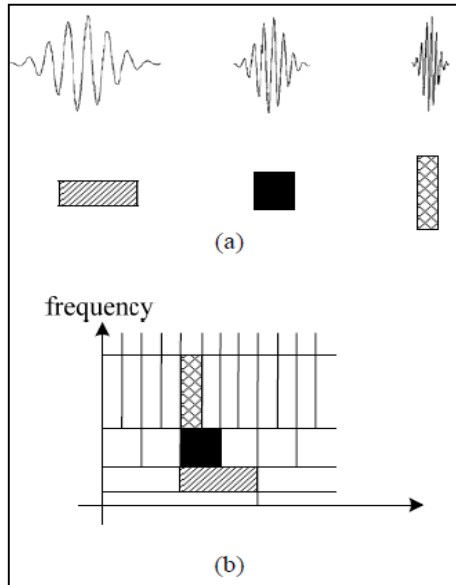


Fig. 2.3 Basis functions and time-frequency resolution of the short-time Fourier Transform (STFT). (a) Basis functions. (b) Coverage of time-frequency plane, (Daubechies, 1988).

In the WT, the time-frequency resolution is different from the STFT, where it is sharper in time at high frequencies, while it is sharper in frequency, at low frequencies, as shown in Fig. 2.4 (b). Such requirement just fits the physical properties of signals (Daubechies, 1988).

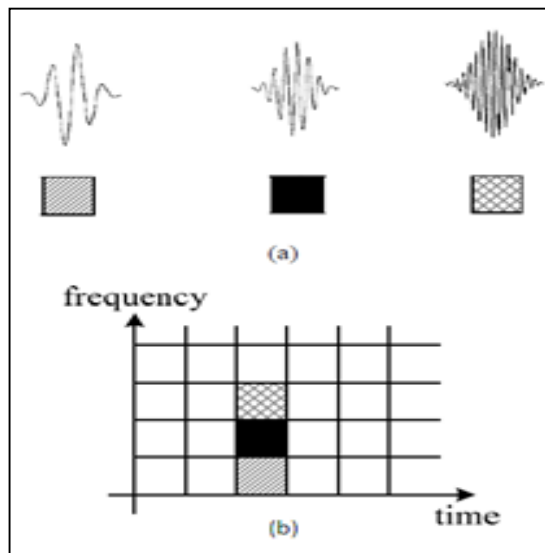


Fig. 2.4 Basis functions and time-frequency resolutions of the wavelet transform (WT). (a) Basis functions. (b) Coverage of time-frequency plane, (Daubechies, 1988).

2.3.2 Discrete wavelet transform

In continuous wavelet transform (CWT), the signals can be analyzed using a set of basic functions which are related to each other by simple scaling and translation. In the form shown so far, the difficulty of using directly properties can be within the CWT. That is the redundancy in the CWT. CWT is calculated by continuously shifting a continuously scalable function $\psi(t)$ over the signal $x(t)$ and calculating the correlation between the two. These scaled functions may not be orthogonal basis. Therefore, the obtained wavelet coefficients will be highly redundant. To overcome this problem, discrete wavelet transforms (DWT) is introduced. DWT is not continuously scalable and translatable but can only be scaled and translated in discrete steps. This is achieved by modifying the wavelet representation to

$$\psi_{j,k}(t) = \frac{1}{\sqrt{s_0^j}} \psi\left(\frac{t - k\tau_0 s_0^j}{s_0^j}\right) \quad (2.10)$$

j and k are integers and $s_0 > 1$ is a fixed dilation step (Combes et al., 2012). The translation factor τ_0 depends on the dilation step. The sampling of the frequency axis corresponds to dyadic sampling as the choosing of $s_0=2$. It is usually selecting that $\tau_0=1$ for the translation factor, it will fulfill the achievement of the dyadic sampling of the time axis, yielding $s=2^j$ and $\tau=k 2^j$. Then it can be written that

$$\psi_{j,k}(t) = \psi_{s,\tau}(t) = \frac{1}{\sqrt{s}} \psi\left(\frac{t - \tau}{s}\right) \quad (2.11)$$

An infinite number of translations and scaling still be desirable even with discrete wavelets to compute the wavelet transform. By not to use an infinite number of discrete wavelets this problem will be processed. A band-pass like spectrum is seen in the wavelet. From Fourier theory, it is also known that compression in time is equivalent to stretching the spectrum and shifting it upwards. This means that a time compression of the wavelet by a factor of 2 will stretch the frequency spectrum of the wavelet by a factor of 2 and also shift all frequency components up by a factor of 2. Using this insight, the finite

spectrum of the signal which used in this thesis can be enclosed with the dilated wavelets spectra as shown in Fig. 2.5.

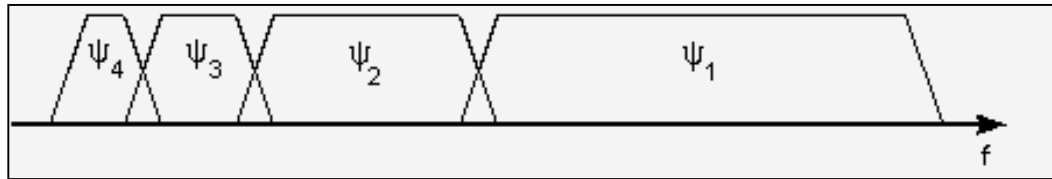


Fig. 2.5 Spectra of dilated wavelets, (Combes et al., 2012).

With a factor of two, every time in the time domain the wavelet is stretched and a half of the bandwidth is produced. In other words, half of the lasting spectrum with every wavelet stretch, is only covered, which indicates that to get the job done, an infinite number of wavelets is required.

With wavelet spectra, not to attempt to cover the spectrum all the way down to zero is basically the solution to this problem. Instead of that when it is small enough then use a cork to plug the hole. This cork then is a low-pass spectrum and it belongs to the so-called scaling function. Mallat (1989) introduced this scaling function. It is sometimes denoted as the averaging filter because of the low-pass nature of the scaling function spectrum. The stage of DWT analysis structure can then be reduced to a half-band two-branch filter bank which can be repeated, after down-sampling by 2, for many finite levels. A reversed structure with up-sampling by 2 and phase-reversed filters can be used for the stage of synthesis. In the case of DWT, digital filtering techniques are used to obtain a time-scale representation for digital signal. The signal can be analyzed by passing it through filters with different cut-off frequencies at different scales (Combes et al., 2012). In numerous practical problems, the discrete nature of the signal that should be analyzed, announces the need to discretize the wavelet transform to use it for sampled discrete signals. Such discretization of the wavelet transform can be met efficiently, by applying recursive filtering stages in iterated filter-banks as shown in Fig. 2.6.

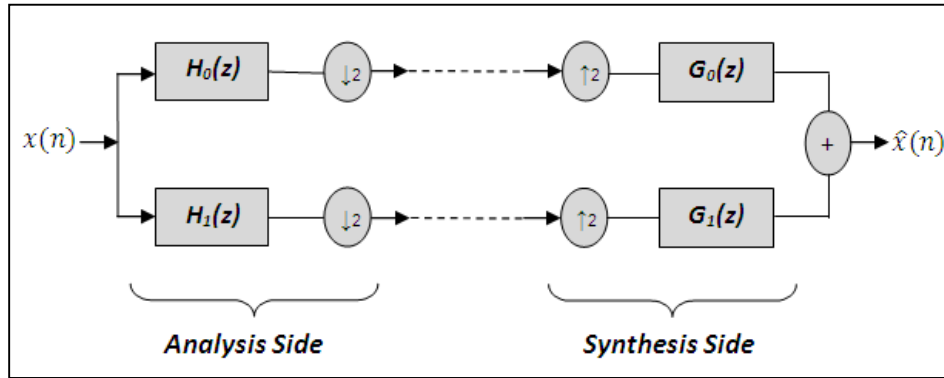


Fig. 2.6 Two-channel quadrature mirror filter banks, (Akansu and Haddad, 2001).

2.4 The Filter Bank

A pair of low-pass and high-pass half-band filters, which satisfy some complementary properties, can compose two-channel filter bank. Each of the two channel signals bandwidth is a half of the bandwidth of the original signal. From this, a half of the original signal sampling rate will be the sampling rate to process the channel signals. A down sampling by two for the channel signals at the output of the analysis bank, and then managed at the lower rate of sampling. Each of the two channel signals must be at start up sampled by two at the signal reconstruction, and then applied to process in the synthesis part of the filter bank.

Two unwanted effects can be caused from the conversion for the sampling rate in the two-channel filter bank: the first from down sampling the aliasing can be resulted, and the second from up-sampling is the imaging can be resulted. Auspiciously, in the synthesis part it can eliminate the aliasing resultant in the analysis part. in the analysis and synthesis part of the two-channel filter banks, choosing the proper combination of filters will achieve that. After eliminating the aliasing effect, the possibility of the nearly perfect (and perfect) reconstruction (NPR and PR) of the original signal can be understood. The perfect reconstruction means that the signal at the output of the filter bank is a delayed replica of the original input signal. The tree-structures where the two-channel filter bank is used as a building block are can be from the widely used and important structures for the two-channel filter banks. In this way, either uniform or non-uniform separation between the channels can give a multi-level multi-channel filter bank (Daubechies, 1988).

Selection of the filter that can be used in discrete wavelet filter banks is the most important role when designing it. Therefore, orthogonal and bi-orthogonal filters is the category of the filter banks types. Symlets, Coiflets, Daubechies and the other of derived FIR wavelet filters, are of perpendicular class. However, these filters are not symmetric and the perpendicular wavelet filters coefficients are real numbers. The high-pass and the low-pass filters do not have the same length in bi- perpendicular FIR wavelet filters, (such as bi- perpendicular 9/7 and bi- perpendicular 5/3). The high-pass filter could be either asymmetric or symmetric while the low-pass filter is always symmetric. The filters coefficients are either integers or real numbers and, a bi-orthogonal filter bank has all even length or all odd length filters, for perfect reconstruction (Chui, 2016).

2.4.1 Quadrature mirror filter (QMF) banks

For many communication and signal processing systems, quadrature mirror filter (QMF) banks have been widely used to realize the goals of sub-band coding and short-time spectral analysis. The QMF bank is used to decompose a signal into sub-bands. These sub-band signals in the analysis system are then decimated by an integer equal to the number of sub-bands. Furthermore, two-channel QMF banks can be used easily for constructing M-channel QMF banks based on a tree structure (Chui, 1992). The two-channel QMF banks, as shown in Fig. 2.6, have received a great interest because of a wide variety of engineering applications. A common requirement in most applications is that the reconstructed signal should be as close to the input signal as possible. In general, the reconstructed signal suffers from three types of error: aliasing error, amplitude distortion, and phase distortion. One of the purposes of QMF designs is to eliminate these three distortions so that the reconstructed signal becomes the exact replica of the original signal with some delay. This is known as perfect reconstruction condition (Akansu and Haddad, 2001).

2.4.2. The analysis and the synthesis filter banks

Analysis filter bank is used to decompose an input signal into sub-bands of the frequency. The two-channel analysis filter bank is shown in Fig. 2.7. Firstly, by passing such $X(z)$ through a high-pass filter $H_1(z)$ and low-pass filter $H_0(z)$ to produce the $U_0(z)$ and $U_1(z)$, respectively, the input signal spectrum $X(z)$ into a low frequency component

$U_0(z)$ and a high frequency component $U_1(z)$ are split (Vaidyanathan, 1993; Fliege, 1994; Strang and Nguyen, 1996).

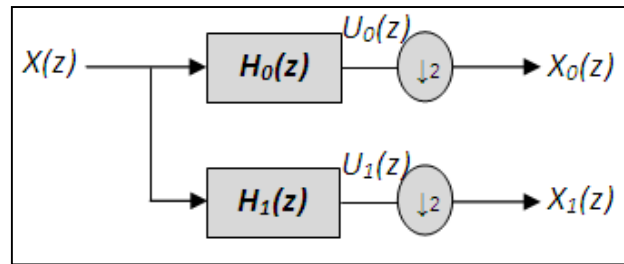


Fig. 2.7 Two-channel analysis filter bank, (Vaidyanathan, 1993).

Accordingly, the available bandwidth from 0 to π with the sampling frequency, $\omega_s = 2\pi$, is divided into two halves, $\pi/2 \leq \omega \leq \pi$ for the high frequency spectrum $U_1(z)$ and $0 \leq \omega \leq \pi/2$ for the lower frequency spectrum $U_0(z)$. Thus, after being passed through the high-pass filters and low-pass respectively, the filtered spectra $U_1(z)$ and $U_0(z)$ passes half the input signal bandwidth. Fig. 2.8 shows the down sampled and filtered signal spectra.

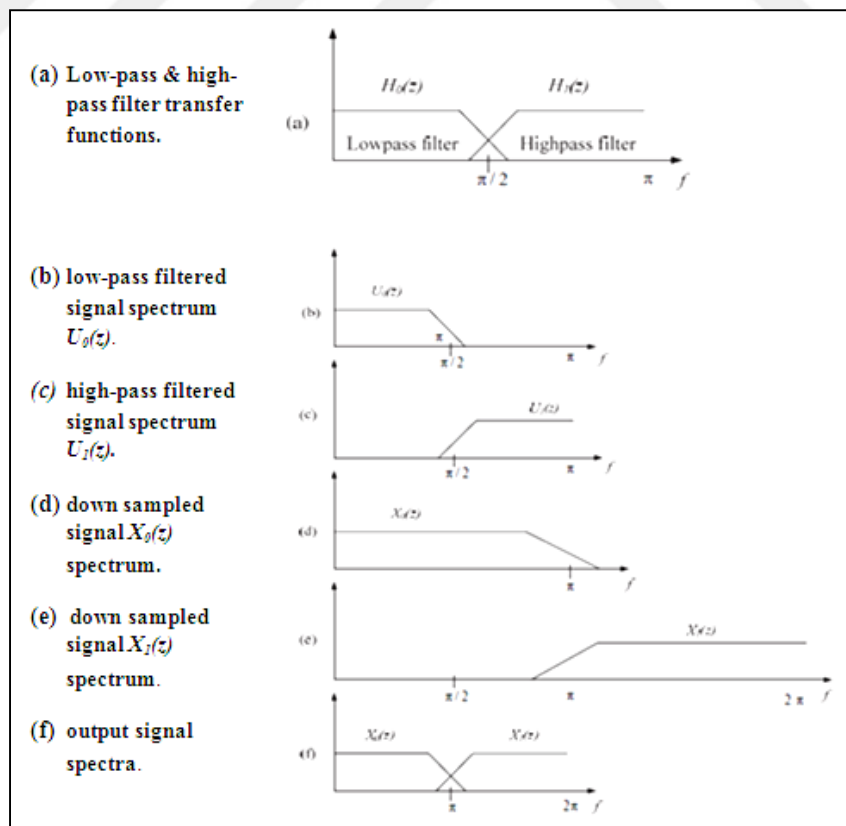


Fig. 2.8 Signal spectra in two-channel analysis filter bank, (Vaidyanathan, 1993).

On the other side, a two-channel synthesis filter bank, shown in Fig. 2.9, contains up-samplers by two to produce signal spectrums $U_0(z)$ and $U_1(z)$. The next step is passing these spectrums through $G_1(z)$ and $G_0(z)$ that denote both high-pass and low-pass filters, and then recombining the up-sampled spectrums $U_1(z)$ and $U_0(z)$ into input signal reconstructed version $\hat{X}(z)$ i.e., the same as the input signal with some delay for perfect reconstruction property (Vaidyanathan, 1993).

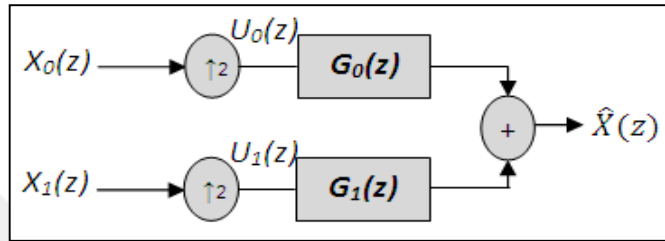


Fig. 2.9 Two-channel Synthesis filter bank, (Vaidyanathan, 1993).

2.4.3. The perfect reconstruction conditions for QMF banks

The analysis and synthesis filters must undertake certain conditions to realize the perfect reconstruction. Let $H_0(z)$ and $H_1(z)$ be the low-pass and high-pass analysis filters, respectively and $G_0(z)$ and $G_1(z)$ are the low-pass and high-pass synthesis filters, respectively.

The synthesis filters $G_0(z)$ and $G_1(z)$ can be obtained depending on the following QMF bank conditions: $H_1(z)=H_0(-z)$, $G_0(z)=H_0(z)$ and $G_1(z)=-H_0(-z)$, that because of existence of the mirror image symmetry (about the frequency $\omega=\pi/2$) between $H_0(e^{j\omega})$ and $H_1(e^{j\omega})$ as shown in Fig. 2.10 (Vaidyanathan, 1993).

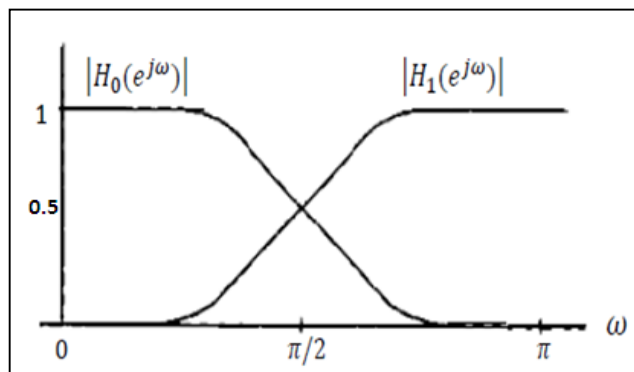


Fig. 2.10 Frequency responses of analysis filters, (Akansu and Haddad, 2001).

To achieve both perfect reconstruction and orthonormality properties, the analysis and synthesis filters must satisfy the following two conditions (Akansu and Haddad, 2001; Srivastava and Maheshwari, 2015):

$$H_0(-z)G_0(z) + H_1(-z)G_1(z) = 0 \quad (2.12)$$

and

$$H_0(z)G_0(z) + H_1(z)G_1(z) = 2z^{-l} \quad (2.13)$$

The first condition represents that the amplitude distortion has a maximum amplitude of one and the second condition represents that the reconstruction is an aliasing-free one. The above conditions can be satisfied in many filters. But especially when the filter coefficients are quantized, accurately wavelet transforms cannot be achieved from all of them. After the reconstruction by calculating the *SNR* of the signal, the accuracy of the wavelet transform can be determined (Srivastava and Maheshwari, 2015).

2.5 Filter Bank for Discrete Wavelet Transform

In signal processing functions, the most widely used applications is filters. Wavelets can be realized by iteration of filters with rescaling. The resolution of the signal, which is a measure of the amount of detail information in the signal, is determined by the filtering operations, and the scale is determined by up-sampling and down-sampling operations (Akansu and Haddad, 2001).

The DWT can be computed by using consecutive low-pass and high-pass filtering of the discrete time-domain signal as shown in Fig. 2.11. In such figure, the input signal is denoted by the sequence $x(n)$, where n is an integer. The low-pass filter is denoted by H_0 while the high-pass filter is denoted by H_1 . At each level, the high-pass filter produces detail information, $d_i(n)$, where i is the level number. rough approximations, $a_i(n)$ and be earned from the association of scaling function with low-pass filter (Vaidyanathan, 1993; Fliege, 1994; Strang and Nguyen, 1996).

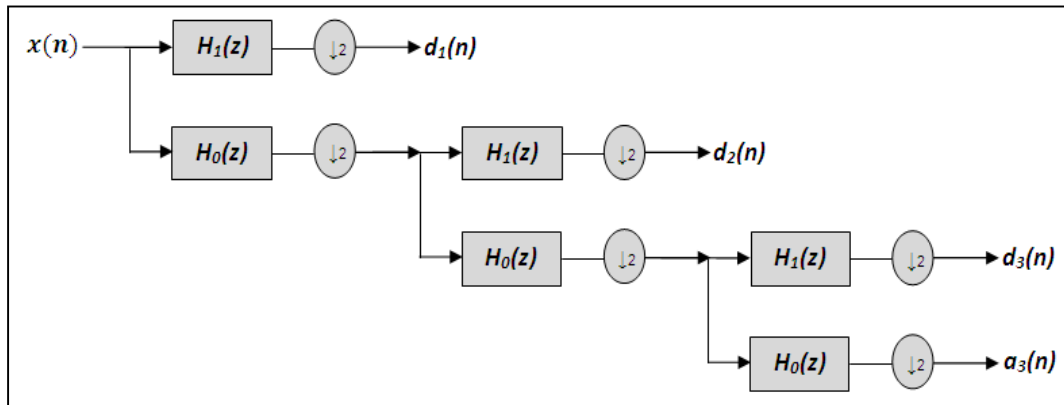


Fig. 2.11 Three-level wavelet decomposition tree, (Vaidyanathan, 1993).

At each decomposition level, the half-band filters produce signals spanning only half the frequency band for the previous level signal. The uncertainty in frequency is reduced by half in other word, this doubles the resolution of the frequency. If the original signal has a highest frequency of B and accordanly to Nyquist's rule, which needs a sampling frequency of $2B$ radians, then it owns now after passing through filters level one, a highest frequency of $B/2$ radians. With the removal of half of the samples number without loss of information at a frequency of B radians, it can now be re-sampled. This is called decimation by 2 which halves the time resolution as the entire signal is now represented by only half of the number of samples. Consequently, the half band low-pass filtering removes half of the frequencies and thus halves the resolution. So the decimation by 2 doubles the scale.

The filtering and decimation processes are continued until the desired level is reached. The length of the signal always determines the maximum number of levels that is needed. The DWT of the original signal is then obtained by concatenating all the coefficients, $a_i(n)$ and $d_i(n)$, starting from the last level of decomposition.

The structure of reconstruction of the original signal from the wavelet coefficients is shown in the Fig. 2.12. Principally, the reverse process of decomposition is the reconstruction. At every level the detail coefficients and approximation are up-sampled by 2, passed through the high-pass and low-pass combination filters and then summed. As in the process of the decomposition, this process is sustained through the same number of levels to gain the original signal. If the analysis filters, H_1 and H_0 , are exchanged with the combination filters, G_1 and G_0 , the Mallat algorithm functions equally positive (Srivastava and Maheshwari, 2015; Chui, 2016).

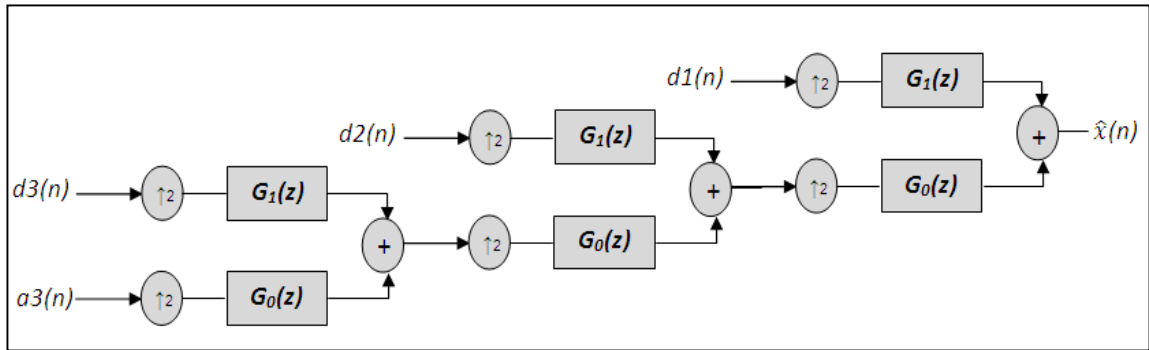


Fig. 2.12 Three-level wavelet reconstruction tree, (Vaidyanathan, 1993).

2.6. Traditional Structures for Discrete Wavelet Transform

There are a variety of structures to implement a filter bank. The followings represent the traditional structures for DWT filter banks (Shukla and Tiwari, 2013):

- 1) structure of Direct form.
- 2) structure of Lifting scheme.
- 3) structure of Lattice.
- 4) structure of Poly phase.

2.6.1. Direct form structure

The structure of direct form can be divided into two parts: followed by decimators, the first part is analysis filter having high-pass and low-pass filters. The second part is the synthesis filters containing up-samplers followed by the low-pass and high-pass filters as shown in Fig. 2.6 (Akansu and Haddad, 2001).

2.6.2. Poly-phase structure

The input signal is split into *even* and *odd* samples in the poly-phase form (decimation by 2 is automatically in the input), correspondingly, a split into *odd* and *even* components in filter coefficients are also happen so that X_{odd} convolves with H_{0odd} of the filter and X_{even} convolves with H_{0even} of the filter. At the end to produce the low-pass

output, the two phases are summed together. For the high-pass filter, the same method is applied where the high-pass filter is split into *even* and *odd* phases H_{1even} and H_{1odd} . The poly-phase analysis operation can be represented by the following matrix equation:

$$\begin{bmatrix} H_{0even} & H_{0odd} \\ H_{1even} & H_{1odd} \end{bmatrix} \times \begin{bmatrix} X_{even} \\ Z^{-1}X_{odd} \end{bmatrix} = H_p(z) \begin{bmatrix} X_{even} \\ Z^{-1}X_{odd} \end{bmatrix} = \begin{bmatrix} Y_0 \\ Y_1 \end{bmatrix} \quad (2.14)$$

In eq. (2.14), the sub-filter H_{0even} and H_{0odd} possess half of the length of the filter H_0 , So, the *even* and *odd* terms are filtered separately by the *even* and *odd* coefficients of these sub-filters. Such sub-filters can operate in parallel to improve speed efficiency. Fig. 2.13 illustrates analysis and synthesis part for poly-phase filter banks (Srivastava and Maheshwari, 2015).

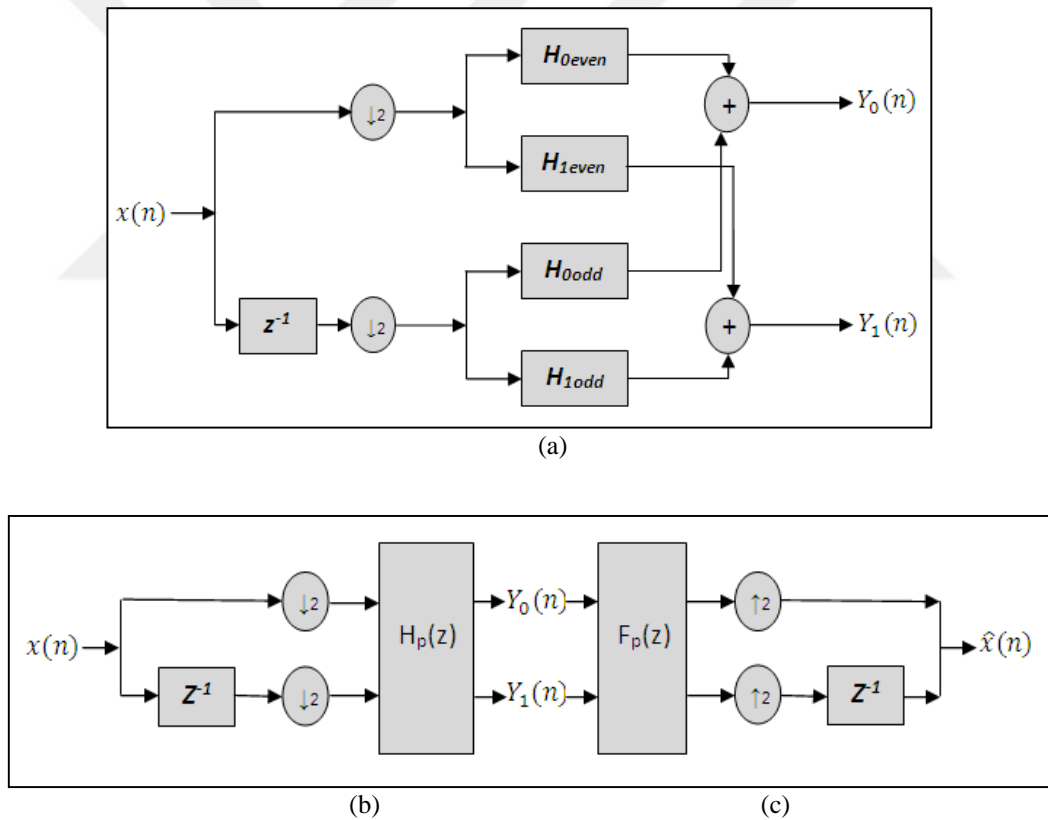


Fig. 2.13 structure of Poly-phase of (a) analysis filter bank (b) equivalent representation of analysis filter bank and (c) synthesis filter bank, (Akansu and Haddad, 2001).

In Fig. 2.13 b and c.

$$H_p(z) = \begin{bmatrix} H_{0even}(z) & H_{0odd}(z) \\ H_{1even}(z) & H_{1odd}(z) \end{bmatrix} \quad (2.15)$$

and

$$F_p(z) = \begin{bmatrix} G_{0even}(z) & G_{1even}(z) \\ G_{0odd}(z) & G_{1odd}(z) \end{bmatrix} \quad (2.16)$$

2.6.3 Lattice structure

$H_p(z)$ can be replaced by a structure of lattice in the poly-phase matrix of eq. (2.15). If the filters $H_1(z)$ and $H_0(z)$ are identified, the filter bank, $H_p(z)$ can be gained. Correspondingly, the structure of lattice can be derived by representing it as a product of simple matrices, if $H_p(z)$ is known. FIR wavelet filter banks can have competently structures of lattice which are easy to implement.

The structure of lattice decreases the multiplications number by reducing the number of resulting coefficients. The structure consists of some design parameters k_i that can be calculated from the FIR filter function and a single overall multiplying factor M . Fig. 2.14 shows the complete structure of lattice for an orthogonal FIR filter bank (Verma and Ali, 2013; Srivastava and Maheshwari, 2015).

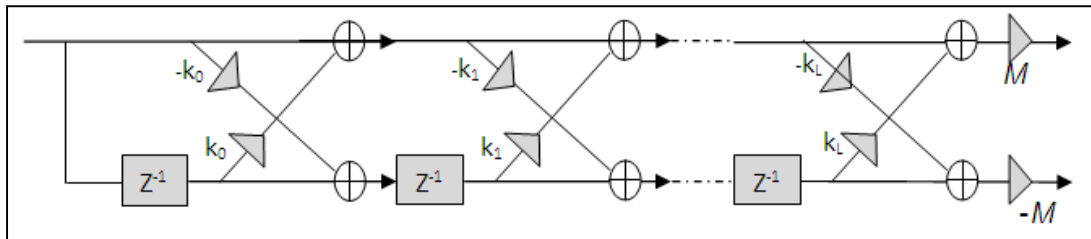


Fig. 2.14 Lattice structure of an orthogonal FIR filter bank, (Fliege, 1994).

2.6.4. Lifting scheme structure

The lifting scheme is shown in Fig. 2.15. It is proposed independently by Herley and Swelden which consists of two steps: dual lifting and lifting step. This structure can be considered the efficient method to construct two-channel filter banks and the fast.

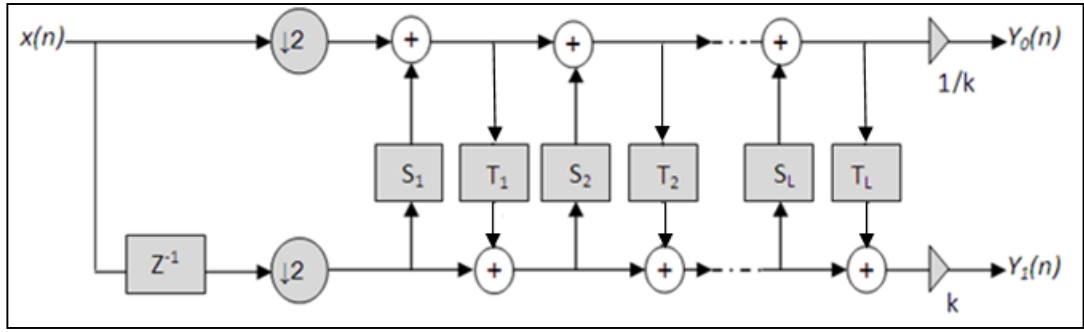


Fig. 2.15 Lifting scheme implementation, (Fliege, 1994).

By using this method, filters with positive properties which fulfill the perfect properties of reconstruction can be built (Akansu and Haddad, 2001). A non-traditional structure is to be designed and implemented in this work utilizing IIR filter banks with lattice all-pass sections.

2.7. All-Pass Filters

In digital signal processing the useful building blocks are all-pass filters that have a nonlinear phase characteristic to construct efficient IIR systems. An all-pass filter $A(z)$ is a system having a constant magnitude response for all the frequencies, *i.e.*,

$$|A(e^{j\omega t})| = c, \quad \text{for all } \omega. \quad (2.17)$$

c : constant.

the group delay distortion or phase equalization without affecting the magnitude response is a strong application of all-pass networks with unit magnitude response. In particular, an important increase of the group delay in the near of the cutoff frequencies can be given from the classical IIR filters. To add extra delay in those frequency ranges is the equalization meaning in this context, where the given characteristic of delay shows low values. The resulting group delay response should be as flat as possible in the pass-band of the filter, so that the signal shape in the time domain can be preserved (Akansu and Haddad, 2001).

The transfer function of an N^{th} -order all-pass filter will be stated in the product form as shown in the following equation:

$$A(z) = \prod_{K=1}^N \frac{z^{-1} - a_K^*}{1 - a_K z^{-1}} \quad (2.18)$$

where a_k , $k = 1, 2, \dots, N$, is a complex number representing the pole of $A(z)$. It is clear from eq. (2.18) that the poles and zeros of the transfer function are reciprocal to each other. To satisfy the stability condition, the poles should be placed inside the unit circle, and consequently the module of a_k is limited with $|a_k| < 1$. Automatically, the transfer function zero being reciprocal to the poles must place out of the unit circle. In fact, by reversing the order of the coefficients, the numerator polynomial can be obtained from the denominator polynomial. For example, a second -order all-pass filter can be represented by the following transfer function (Akansu and Haddad, 2001):

$$A_{AP}(z^2) = \frac{a_2 + a_1 z^{-1} + z^{-2}}{1 + a_1 z^{-1} + a_2 z^{-2}} \quad (2.19)$$

2.8. FIR and IIR Wavelet Filter Banks

The FIR wavelet filters are usually utilized in the design of the wavelet filter banks, but it is well known that these filters haven't high frequency discrimination. To increase the discrimination properties for such FIR filters, their order must be increased, but this will in turn increase the implementation complexity and time delay. As a solution, the highly discriminative IIR wavelet filter banks that have less implementation complexity and less time delay which can be proposed instead of the classical FIR wavelet filter banks.

Recursive filter algorithms are required to realize such IIR filters. A class of recursive filters that can be implemented with a guaranteed stability is wave digital filters (Akansu and Haddad, 2001).

2.8.1. Two-channels QMF banks using all-pass filters

It has been shown that using a two-channel QMF banks can eliminate both aliasing error and amplitude distortion completely. The IIR wavelet filter banks can be designed composing two all-pass filters (this circuit is considered as the best kernel for building up

a multi-channel IIR filter banks). Fig. 2.16 shows the based IIR QMF banks two-channel all-pass filter (Akansu and Haddad, 2001).

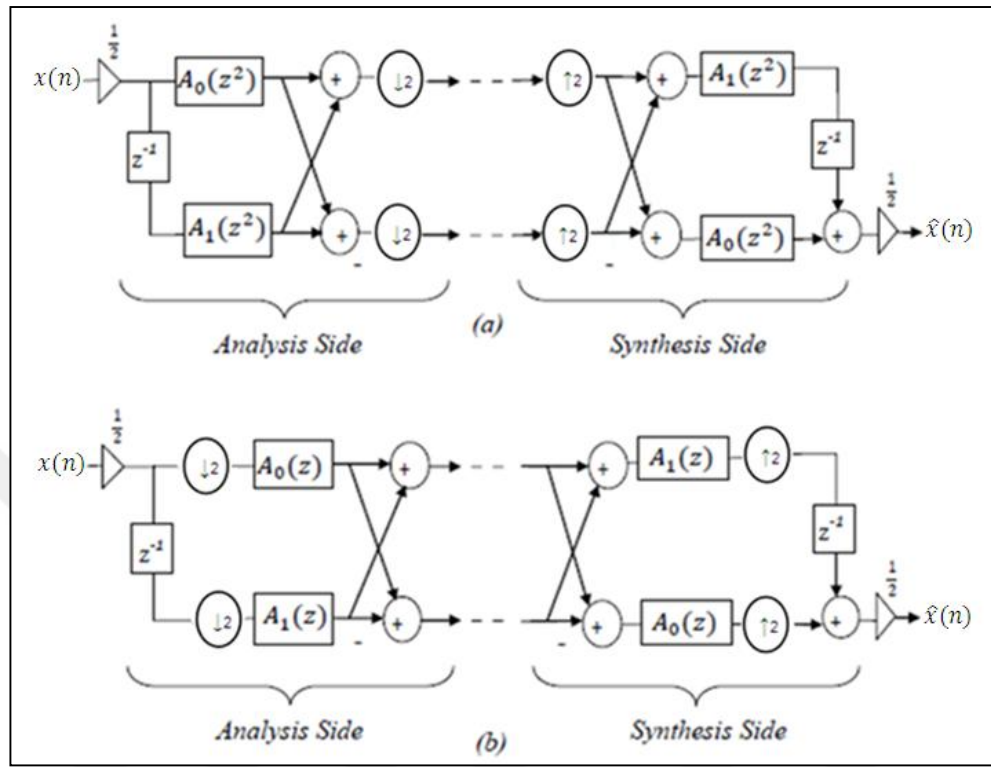


Fig. 2.16 Lattice structure realization of the IIR wavelet filter bank. (a) Direct lattice structure realization. (b) Computationally efficient realization, (Akansu and Haddad, 2001).

A branch-interchange method is applied in the two all-pass sections of analysis and synthesis sides to remove the phase distortion (Akansu and Haddad, 2001). As shown in Fig. 2.17 a modified stable linear phase structure can also be derived.

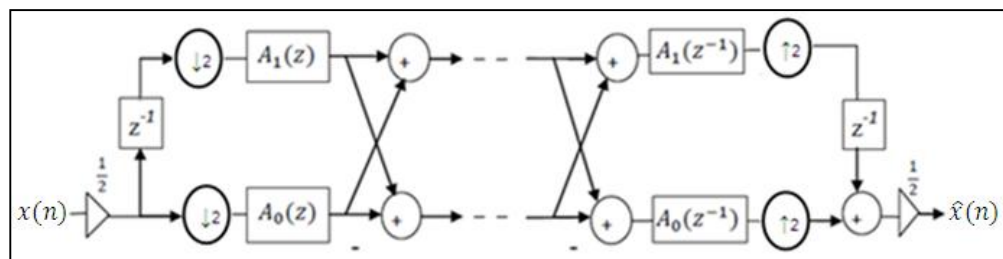


Fig. 2.17 The modified lattice structure realization of the IIR wavelet filter bank, (Akansu and Haddad, 2001).

In this work, the design of two-channel linear-phase QMF banks constructed using real IIR digital all-pass filters is considered. The design problem is appropriately formulated to result in a simple optimization problem. Using both intermediate filter design and Gazsi method (Abdul-Jabbar, 2011), to find the real coefficients for the IIR digital all-pass filters, the optimization problem can be efficiently solved through equating the numerator of the transfer function of the bi-reciprocal lattice wave digital filter with the numerator that resulting from the transfer function of intermediate filter. The resulting two-channel QMF IIR filter banks possess approximate linear-phase response without magnitude distortion; that is the main advantage of using all-pass sections (Chui, 1992).

2.8.2 IIR wavelet filter banks

When using lattice structure with all-pass sections of the types shown in Figs. 2.16 and 2.17, a all-pass filter-based IIR QMF banks with two-channel can be represented by a very efficient way. In Fig. 2.16 the components of lattice are the second-order all-pass filters $A_0(z^2)$ and $A_1(z^2)$ with the following transfer functions (Akansu and Haddad, 2001):

$$A_0(z^2) = \prod_{i=2,4}^{(N+1)/2} \frac{\alpha_i + z^{-2}}{1 + \alpha_i z^{-2}} \quad (2.20)$$

And

$$A_1(z^2) = \prod_{i=3,5}^{(N+1)/2} \frac{\alpha_i + z^{-2}}{1 + \alpha_i z^{-2}} \quad (2.21)$$

where α_i is the multiplier coefficient value in the i^{th} all-pass section.

Let $G_I(z)$ and $G_0(z)$ denote the transfer functions of the high-pass and low-pass filter of the combination part and let $H_I(z)$ and $H_0(z)$ denote the transfer functions of the high-pass and low-pass filter of the analysis part of the QMF bank with two-channel. For the low-pass side, the analysis filters $H_I(z)$ and $H_0(z)$ can be written as (Akansu and Haddad, 2001):

$$H_0(z) = \frac{1}{2} [A_0(z^2) + z^{-1}A_1(z^2)] \quad (2.22)$$

and for the high-pass side as

$$H_1(z) = \frac{1}{2}[A_0(z^2) - z^{-1}A_1(z^2)] \quad (2.23)$$

2.9. Wave Digital Filters (WDFs)

Wave digital filters (WDFs) are well known to have many advantageous properties. Such properties include low coefficient sensitivity, good dynamic range, and especially, good stability properties, under different quantization levels (Shukla and Tiwari, 2013). WDFs comprise a eclectic class of IIR digital filters that are well appropriate for implementation. The lattice wave digital filter is the most attractive one among different wave digital filters. All WDFs have their corresponding filters in the analogue reference domain. Inherit of several fundamental properties, WDFs are derived from analog reference filters. If the reference filter has a low sensitivity to variation in element values, which is the case for certain RLC filters, the digital filter can be inherit this property (Shukla and Tiwari, 2013). One more property inherited from the reference filter is the stability for the filter through implementation. Richards' structures and ladder structures are examples of structures of WDF, fitting for implementation. Though, lattice WDFs (LWDFs) is a class of WDFs that is even more suitable for VLSI implementation. From analog lattice filters, these filter structures are derived.

The type of IIR filters that well suit the implementation on FPGA is the lattice wave digital filter (LWDF) (Shukla and Tiwari, 2013).

2.9.1. Lattice wave digital filters (LWDFs)

Where each branch realizes an all-pass filter, an LWDF is a parallel structure of two-branch as shown in Fig. 2.18. There are several methods to appreciate LWDFs. One of the most striking method, as shown in Fig. 2.19, is to use cascaded first-order and second-order sections. By using symmetric parallel adaptors or two-port series, the second-order and first-order sections are realized with certain equivalence transformations. By using three-port series- or parallel adaptors, the second-order sections can also be realized (Abdul-Jabbar, 2009; 2011).

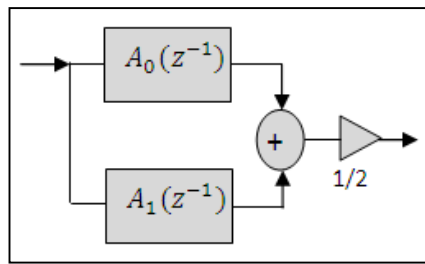


Fig. 2.18 Lattice wave digital filter block diagram, (Abdul-Jabbar, 2009).

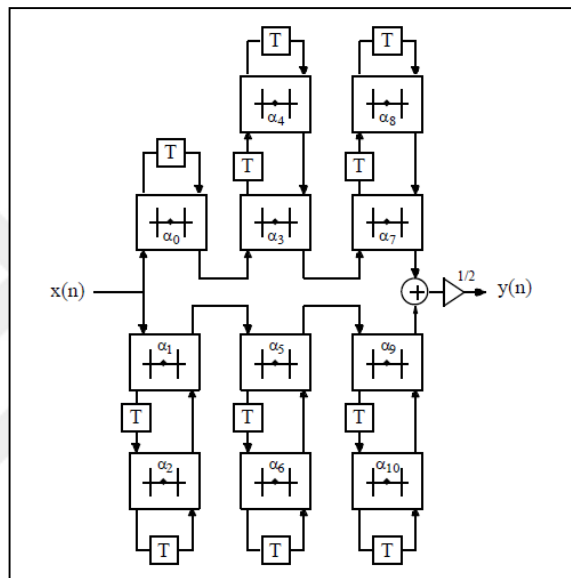


Fig. 2.19 An 11th-order lattice wave digital filter (Abdul-Jabbar, 2009).

The LWDF structure inherits some properties from the reference filter (the analog lattice filter), the low-pass-band sensitivity and high stop-band sensitivity. The LWDF structure is well appropriate for VLSI implementation because it is highly modular yielding a high degree of parallelism. By using symmetric two-port adaptors, the all-pass filters are composed of cascaded second-order and first-order Richards' structures implemented. The signal-flow graph of the symmetric two-port adaptor is shown in Fig. 2.20 (Abdul-Jabbar, 2009; 2011).

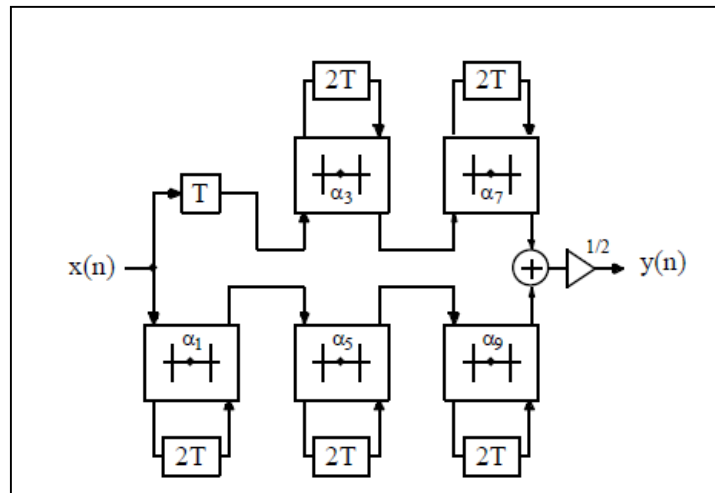


Fig. 2.20 A symmetric two-port adaptor, (Akansu and Haddad, 2001).

2.9.2. Bi-reciprocal lattice wave digital filters (BLWDFs)

A sub-class of LWDFs is bi-reciprocal LWDFs (BLWDFs). The magnitude function of a BLWDF is anti-symmetric around $\pi/2$. Comparing the BLWDF to the LWDF of the same filter order, more than half of the coefficients of the first are zeros (Abdul-Jabbar, 2009). Fig. 2.19 (for an 11th -order structure) can then be modified to BLWDF structure as shown in Fig. 2.21. This conversion will reduce the arithmetic complexity of the BLWDF implementation as well as increase the throughput, compared to an LWDF implementation (Abdul-Jabbar, 2011). Moreover, when the application is in a decimator or interpolator by a factor of 2, the filter can run at the lower sampling rate (Abdul-Jabbar, 2009).

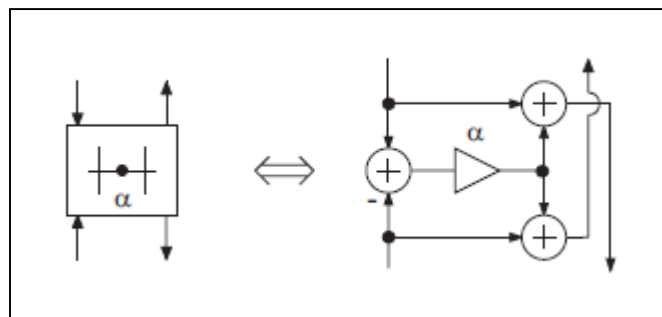


Fig. 2.21 An 11th -order bi-reciprocal LWDF, (Johansson and Wanhammar, 1996).

The transfer function to the low-pass filter of a bi-reciprocal LWDF can be written as (Johansson and Wanhammar, 1996; Abdul-Jabbar, 2009):

$$H(z) = \frac{1}{2} [A_0(z^2) + z^{-1}A_1(z^2)] \quad (2.24)$$

where the transfer function $A_0(z^2)$ corresponds to the lower branch in Fig.(2-22) while $A_1(z^2)$ corresponds to the upper (Abdul-Jabbar, 2009).

The frequency response of the filter can be written as

$$H(e^{j\omega T}) = \frac{1}{2} (e^{j\Phi_0(\omega T)} + e^{j\Phi_1(\omega T)}) \quad (2.25)$$

Where

$$\Phi_k(\omega T) = -k\omega T + \arg\{H_k(e^{j\omega T})\}, \quad k = 0,1 \quad (2.26)$$

is the phase response of the k^{th} branch and T is the sampling period. The magnitude of the overall filter is hence restricted by

$$|H(e^{j\omega T})| \leq 1 \quad (2.27)$$

The BLWDF transfer function and its complementary transfer function are power complementary functions. So, BLWDFs have the following relationships:

$$|H(e^{j\omega T})|^2 + |H(e^{j(\omega T - \pi)})|^2 = 1 \quad (2.28)$$

which means that the pass-band and stop-band edges (ω_c & ω_s , respectively) are related

by $\omega_c T + \omega_s T = \pi$.

to define the principles of the transmission zeros and the attenuation zeros, the following discussions are achieved. On the unit circle in the z -plane, these zeros always arise. Which the magnitude function reaches to its maximum value, an attenuation zero represents to an angle $\omega_0 T$ at. In the BLWDFs this takes place when

$$|H(e^{j\omega_0 T})| = 1 \quad (2.29)$$

At which the magnitude function is zero, a transmission zero represents to an angle $\omega_1 T$, *i.e.*, when

$$|H(e^{j\omega_1 T})| = 0 \quad (2.30)$$

It follows from eq. (2.27) if the filter has an attenuation zero at $\omega_0 T$, then that it also has a transmission zero at $\pi - \omega_0 T$.

The phase manners of an ideal poly-phase network must approximate the phase responses of the overall branch transfer functions to get a low-pass filter. The phase responses of both branches must have the same value at an attenuation zero, *i.e.*,

$$\Phi_0(\omega_0 T) = \Phi_1(\omega_0 T) \quad (2.31)$$

Hence, the phase responses must be approximately equal in the filter pass-band. the difference in phase between the two branches must be at a transmission zero

$$\Phi_0(\omega_1 T) - \Phi_1(\omega_1 T) = \pi \quad (2.32)$$

Thus, the difference in phase between the two branches must approximate π in the stop-band of the filter. the degrees of $A_0(z^2)$ and $A_1(z^2)$ must differ only by one to make sure that only one stop-band occur and one pass-band, (Abdul-Jabbar, 2009).

2.10. Literature Review

Many attempts were accomplished to de-noising noisy images, resulting in a wide variation in the output de-noised image performances.

In 2007, By using lifting schemes architectures for 2-D and 1-D discrete wavelet transform (DWT) were presented (Xiong et al., 2007). To optimize the architecture for 1-D DWT, an embedded decimation technique was exploited, which was designed to receive an input and generate an output with the low- and high-frequency components of original data being available alternately. By employing parallel and pipeline techniques, based on the 1-D DWT lifting scheme architecture was extended to an efficient line-based architecture for 2-D DWT. Such techniques were mainly composed of one vertical filter

module and two horizontal filter modules, working in parallel and pipeline fashion with 100% hardware utilization. Two 2-D fast architectures were presented. They can perform J levels of decomposition for $(N * N)$ -sized image in approximately $2N^2(1 - 4^{-J})/3$ internal clock cycles. In tradeoff among hardware cost, throughput rate, output latency and control complexity, the lifting scheme architectures for 2-D DWT were proved to be efficient alternatives, compared with some other works reported in previous literature,.

In many other wavelet-based techniques, it has been proved that these techniques can offer good processing quality and best flexibility for the problem of noise in both 1-D signals & 2-D images. Noise-existence in image processing and applications is practically one of the most important problems to solve because it affects the overall performance of the imaginary systems. Therefore, various methods were developed by Turkish authors for de-noising. In 2007, Vatansever et al. (2002) presented a comparison of some wavelet de-noising methods with some recent methods, highlighting some of wave transform properties. Also in 2007, M. İkiz et al. (2007) suggested a classification system used to recognize the speaker identity by means of wavelet analysis and neural network approach. After sampling, the 1-D voice signals generated from 10 different persons (6 males and 4 females) were de-noised using Wave-flow and Wave-pad shareware programs. A Matlab Simulink model was designed to generate the tested data from the voice signals. This data was applied once again as an input signal for a Matlab-based neural network to classify the voice data into different speakers. Again in 2007, Demir and Erturk (2007) proposed a hyperspectral image classification approach using support vector machines (SVM) after a wavelet de-noising. The noise reduction was carried out in each band independently. Compared with direct SVM based classification, it was shown that the SVM classification of de-noised images can result in significantly better classification accuracy, improved sparsity and faster testing time. Such properties make the wavelet de-noised SVM based hyperspectral classification approach more suitable for low-complex and real-time applications.

In 2010, based on the Haar wavelet transform a de-noising algorithm was presented by a non-Turkish. By using the Tetrolet transform the methodology was based on an algorithm initially developed for compression of image. An adaptive Haar wavelet transform whose support is tetrominoes that is basically called The Tetrolet transform, that is, shapes made by connecting four equal sized squares. By an additive white Gaussian noise (AWGN) with the assumption of universal hard thresholding, and over the classical Haar wavelet transform, that algorithm gave 2.5 dB improvement in PSNR

for some de-noised test images corrupted previously. By such algorithm, on each 4x4 block of the image, it had been shown that the algorithm was local and can work independently. In addition, the algorithm was well suited for efficient hardware implementation because of its local nature and the simplicity of its computations (Singh, 2010).

Back to Turkish authors, Ergen and Baykara (2011) gave a comparison between the wavelet and wavelet package decomposition for image de-noising. They examined many standard test images and their results showed that increasing of decomposition depth has no effect on improving the values of peak signal- to-noise ratio (PSNR). They concluded that wavelet decomposition is superior to wavelet package decomposition and more suitable to be used in image de-noising. In addition, the performances of wavelet de-noising methods were examined in 2012 by Ergen (2012) for several variations including various rules of thresholding with different types of wavelet filters. Comparisons were accomplished for the three estimation methods of threshold with different wavelet types. Results have shown that rather than the wavelet type, the most important controlling factor in wavelet de-noising is decomposition level. It has been shown that neither the estimation of threshold value nor the threshold type has any effect on the de-noising quality. However, no worthy differences in the resulting de-noised images were seen till the 6-level decomposition, after such level, a better performance in terms of SNR level for Rigrisure method was achieved over the others. Also, it was shown that the decomposition level was absolutely dependent on the frequency band of the image to be analyzed and its sampling frequency and for large oscillation numbers the wavelet type was not very important. one of the major application areas of communication systems is constituted in Radar. The noise may be mixed with the original signal because of human-induced or environmental reasons, while radar signal passes from source to target. Hence, it may be impossible to read the radar signal correctly because of that noise. a non-traditional wavelet packet transform (WPT) for the de-noising of weak radar signals with high-performance has been suggested in 2014 by Üstündağ et al. (2014). By applying the genetic algorithm (GA) structure as an intelligent system for optimization the appropriate wavelet family type while such non-traditional WPT transform were performed, decomposition level number and entropy type were instantaneously selected. Furthermore, by using the fuzzy s-function as a thresholding function and variable parameters of this function were set according to the best performance criteria, the suitable threshold function was selected. in the literature for de-noising of the weak radar

signals, the method was then compared with other algorithms available. Using root mean square error and the correlation coefficient criteria as metrics, the system performance was tested. Results highlighted that the suggested method gave better performance evaluations than the other de-noising methods available in the literature. Recently, in 2015, Srivastava and Maheshwari (2015) presented a work that reviewed and summarized the use of wavelet transform for de-noising of signals contaminated with noise. Their work also discussed the diverse applications of the wavelet transform.

With special emphasis in image de-noising in non-Turkish paper, Mastriani (2015) presented quantum Boolean image processing methodology. Two new interfaces of an approach for internal image representation was highlighting and presented: quantum-to-classical and classical-to-quantum. Working exclusively with computational basis states (CBS) the image de-noising was called quantum Boolean mean filter. The image was decomposed into its three color components (red, green and blue) in that sense. Then, for each color (with 8 bits per pixel), the bit-planes were obtained, *i.e.*, 8 bit-planes per color. By using the most significant bit (MSB) bit-plane of each color, exclusive manner, all operations were accomplished. a quantum Boolean version of the image was achieved within the quantum machine, after a classical-to-quantum interface (which included a classical inverter). The methodology prevented the problem of quantum measurement, which alters the results of the measured except in the case of CBS. By proceeding to reassemble each color component, the results of filtering the inverted version of MSB, inside quantum machine, were passed through a quantum-to-classical interface (which involves another classical inverter). Finally, by filtering the image and discussing some appropriate metrics for image de-noising in a set of experimental results, this processing methodology was concluded. Such metrics include the correlation factor and Peak signal-to-noise ratio (PSNR). It had been shown that the results of such quantum Boolean de-noising methodology were superior to those obtained by the classical techniques.

3. THE PROPOSED METHODOLOGY AND EFFICIENT REALIZATION

In this chapter, a two-dimensional (2-D) circular-support wavelet transform (2-D CSWT) is introduced. A 2-D CSWT is simulated in forms of 2-D frequency- mask filter bank and introduced for de-noising of noisy images. A de-noising scheme via frequency masking realization of the overall filter bank is presented. Then, such overall structure is modified into some efficient one.

3.1. 2-D Circular-Support Wavelet Transform (2-D CSWT)

The 2-D CSWT is a geometrical image transform which was presented recently in 2013, Abdul-Jabbar et al. (2013) depending on the idea of 2-D elliptical-support wavelet filter bank (Abdul-Jabbar and Abdulkader, 2012). 2-D CSWT can efficiently represent images using 2-D circular spectral split schemes (circularly-decomposed frequency subspaces (Abdul-Jabbar and Abdulkader, 2010)). The classical one-dimensional (1-D) analysis Haar filter bank branches which are simulated as a parallel connection of both low-pass and high-pass filters, can be transformed into their 2-D counterparts. The designed 2-D circular wavelet filter bank branches can be easily realized by their frequency-masks. The proposed scheme consists of two parts as in the Figs. 3.1 and 3.2. They can be simulated using a Matlab program to obtain the low and high frequency coefficients (on two separable 2-D regions). As shown in the Fig. 3.1, a 3-level (or even more) 2-D circular decomposition stage with down-sampling by (2, 2) can be achieved, resulting in reducing the scales of the 2-D circular-splitting regions by a quarter at each decomposition scale. The input noisy image is decomposed by such 2-D CSWT transform into $(r + 1)$ low- and high-pass coefficients, where r is the number of the decomposition level.

3.2. 2-D Circular-Support Wavelet Transform for Image De-noising

For the process of image de-noising, the decomposition stage of the 2-D CSWT can be adopted (as shown in Fig. 3.1) with some thresholding processes being applied on all high-pass coefficient channels. Different thresholding levels (Th1, Th2, and Th3) can be applied to maintain as much as possible noise-free high-pass channels.

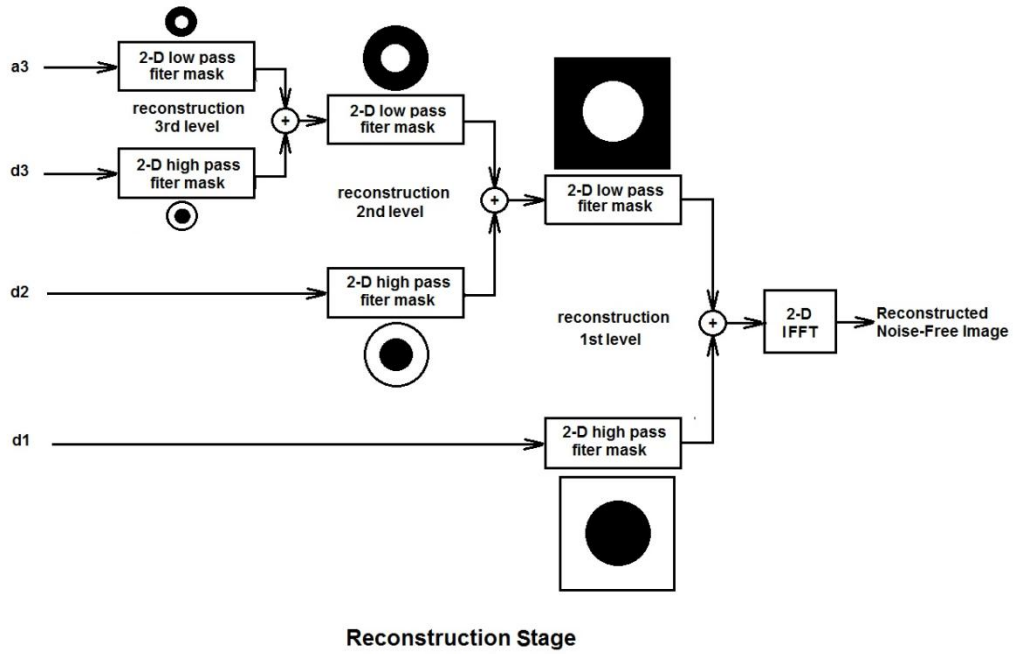


Fig. 3.1 3-level decomposition stage of the proposed de-noising scheme with thresholding.

The de-noised image can result from the 2-D circular-support reconstruction filter bank which is shown also in the Fig. 3.2 as a reconstruction stage of the 2-D CSWT. In this stage, up-sampling by (2, 2) can be applied at each level to have the same size of the original image at the output.

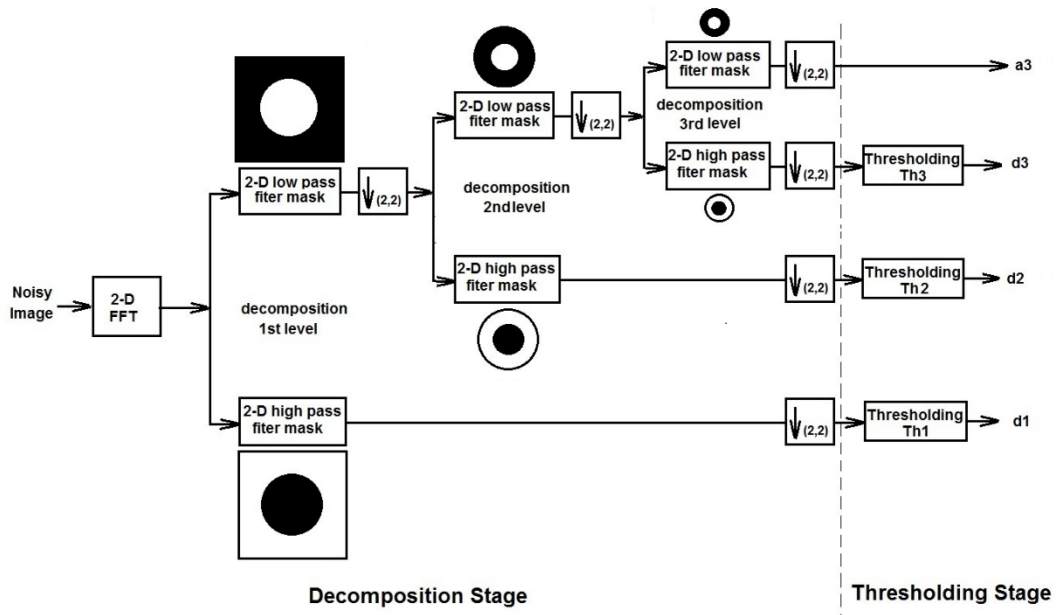


Fig. 3.2 3-level reconstruction stage the proposed de-noising scheme.

3.3. Efficient and Simplified Structures

Some efficient and simplified structures of the 3-level 2-D circular decomposition and reconstruction stages in Figs. 3.1 & 3.2 are proposed and shown in Figs. 3.3 & 3.4, respectively. It is believed that such structures Figs. 3.3 & 3.4 are more efficient in the sense of the required processing time. They are also simplified in the sense of realization as compared to those given in Figs. 3.1& 3.2. A 3-level simplified decomposition stage with thresholding is shown in Fig. 3.3, while the corresponding 3-level simplified reconstruction stage is shown in Fig. 3.4.

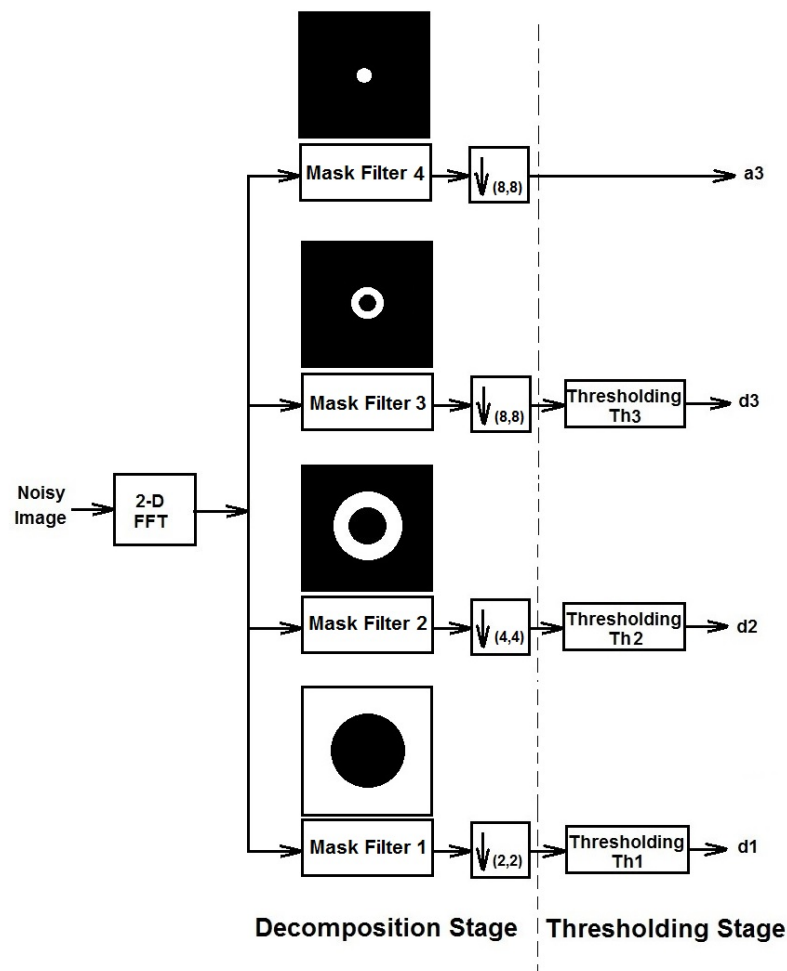


Fig. 3.3. A 3-level simplified decomposition stage of the simplified de-noising structure with thresholding.

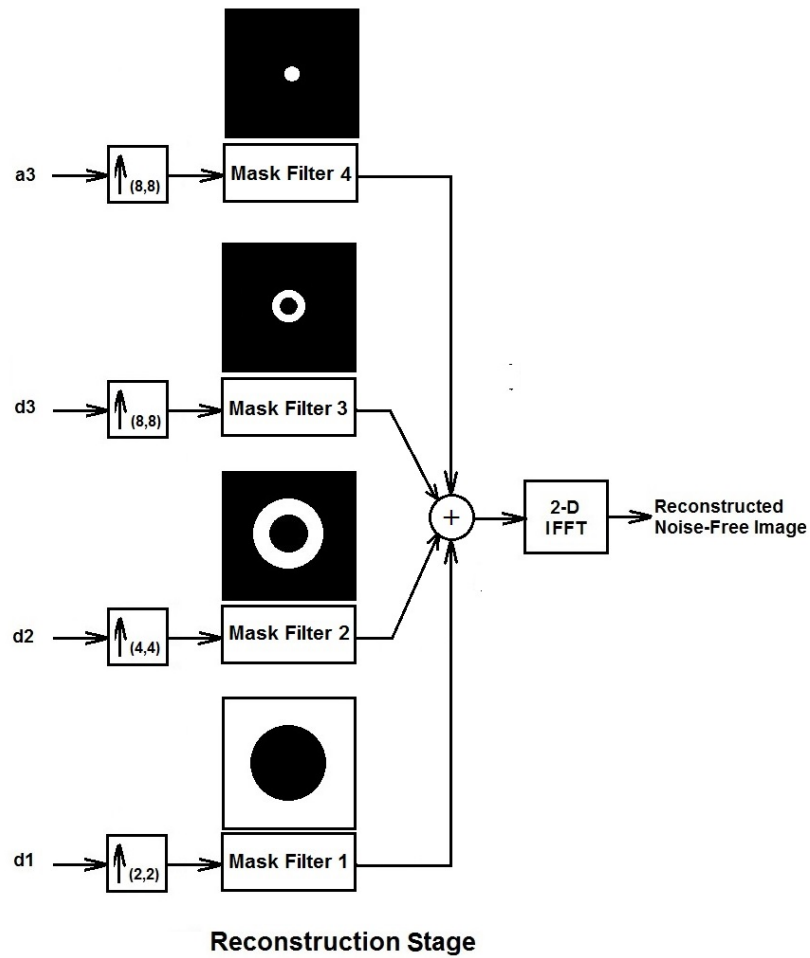


Fig. 3.4 The corresponding 3-level simplified reconstruction stage of the simplified de-noising structure.

The above 3-level simplified structures for decomposition and reconstruction are to be applied in this thesis for image de-noising and they will be tested in the next chapter.

4. TEST RESULTS

In this chapter, the performance of the proposed de-noising scheme in the previous chapter is evaluated by examining such scheme with many standard test noisy-images. The resulting reconstructed images of the proposed de-noising scheme with circular wavelet in Figs. 3.3 & 3.4 is then compared with their counterparts of the classical 2-D wavelet de-noising scheme to highlight the performance superiority of the proposed. Five noisy images (namely; Camera man, Barbara, Lena, Boat and House) are tested with three different levels of noise. The noise will be in two types (Gaussian salt & pepper). The evaluation assessments are given in terms of the correlation factor (Correlation) and the peak-signal-to-noise ratio (PSNR) in dB.

4.1. Results of circular wavelet de-noising by thresholding

The proposed circular wavelet de-noising scheme is tested in this section on the above mentioned testing five noisy images with three different levels of Gaussian noise and another three different levels of Salt and pepper noise. We will start in the next sub-section with the results obtained by examination of three different levels of Gaussian noise.

4.1.1. Results of circular wavelet de-noising by thresholding

In this sub-section, the performance of the proposed circular wavelet de-noising scheme is evaluated via the above mentioned testing five noisy images. Three levels of Gaussian noise are used in that evaluation. These levels of Gaussian noise are low-level noise with variance = 0.001, mid-level noise with variance = 0.01 and high-level noise with variance = 0.1. The noisy Camera man image with low-level Gaussian noise; variance = 0.001 & mean = 0 is shown in Fig. 4.1 (a). The corresponding reconstructed Camera man image using circular wavelet de-noising scheme is shown in Fig. 4.1 (b) with Correlation = 0.9808 and PSNR = 26.4181 dB.



(a)



(b)

Fig. 4.1 (a) Noisy Camera man image with low-level Gaussian noise; variance = 0.001 & mean = 0, (b) The corresponding reconstructed Camera man image using circular wavelet de-noising scheme; Correlation = 0.9808 and PSNR = 26.4181 dB.

The noisy Camera man image with mid-level Gaussian noise; variance = 0.01 & mean = 0 is shown in Fig. 4.2 (a). The corresponding reconstructed Camera man image using circular wavelet de-noising scheme is shown in Fig. 4.2 (b) with Correlation = 0.9738 and PSNR = 24.9231 dB.



(a)



(b)

Fig. 4.2 (a) Noisy Camera man image with mid-level Gaussian noise; variance = 0.01 & mean = 0, (b) The corresponding reconstructed Camera man image using circular wavelet de-noising scheme; Correlation = 0.9738 and PSNR = 24.9231 dB.

The noisy Camera man image with high-level Gaussian noise; variance = 0.1 & mean = 0 is shown in Fig. 4.3 (a). The corresponding reconstructed Camera man image is shown in Fig. 4.3 (b) with Correlation = 0.9245 and PSNR = 20.0761 dB.

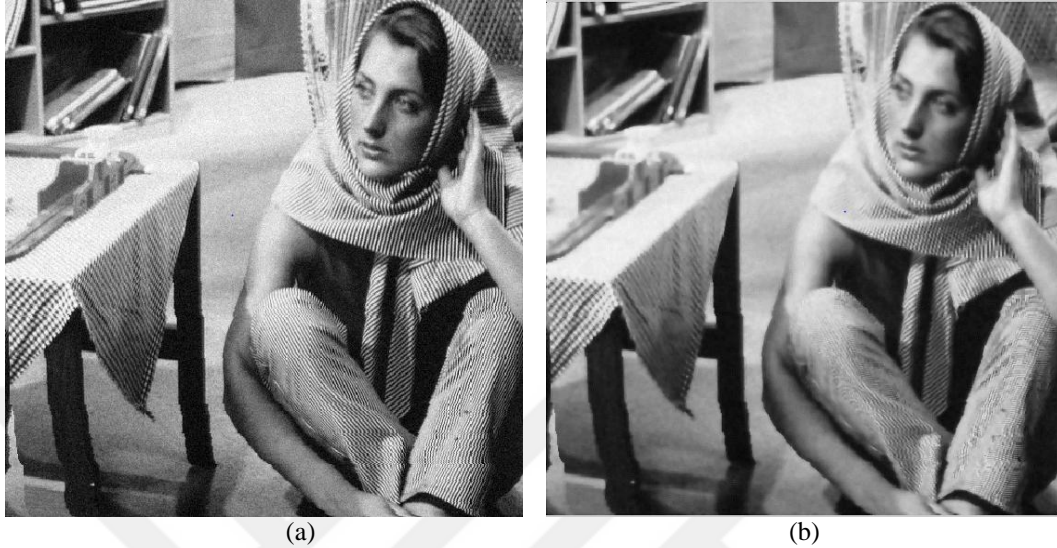


Fig. 4.3 (a) Noisy Barbara image with high-level Gaussian noise; variance = 0.1 & mean = 0, (b) The corresponding reconstructed Camera man image using circular wavelet de-noising scheme; Correlation = 0.9245 and PSNR = 20.0761 dB.

The noisy Barbara image with low-level Gaussian noise; variance = 0.001 & mean = 0 is shown in Fig. 4.4 (a). The corresponding reconstructed Barbara image using circular wavelet de-noising scheme is shown in Fig. 4.4 (b) with Correlation = 0.9644 and PSNR = 22.5153 dB.

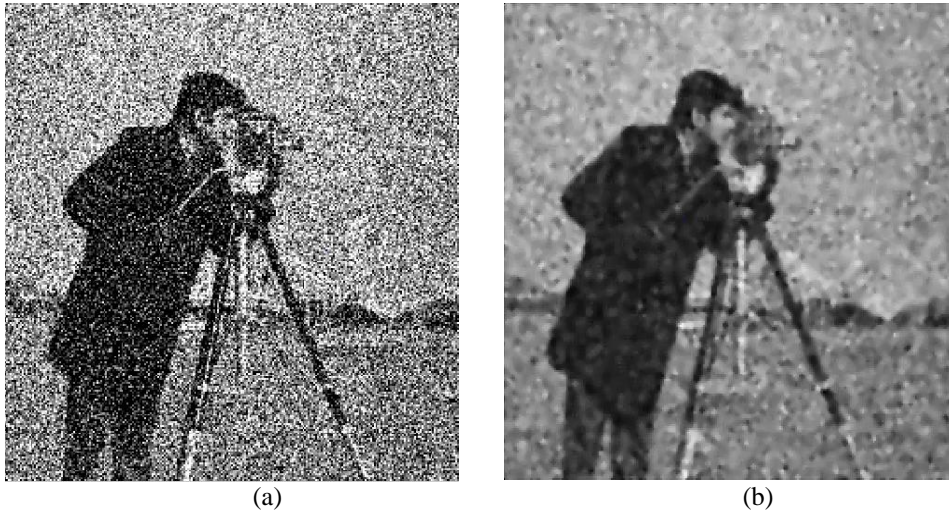


Fig. 4.4 (a) Noisy Camera man image with low-level Gaussian noise; variance = 0.001 & mean = 0, (b) The corresponding reconstructed Camera man image using circular wavelet de-noising scheme, Correlation = 0.9644 and PSNR = 22.5153 dB.

The noisy Barbara image with mid-level Gaussian noise; variance = 0.01 & mean = 0 is shown in Fig. 4.5 (a). The corresponding reconstructed Barbara image using circular wavelet de-noising scheme is shown in Fig. 4.5 (b) with Correlation = 0.9571 and PSNR = 21.6654 dB.

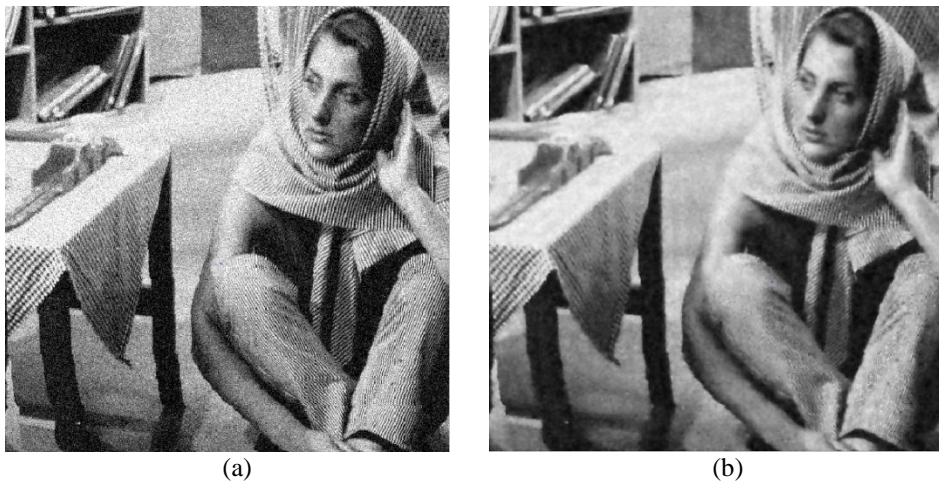


Fig. 4.5 (a) Noisy Barbara image with mid-level Gaussian noise; variance = 0.01 & mean = 0, (b) The corresponding reconstructed Barbara image using circular wavelet de-noising scheme; Correlation = 0.9571 and PSNR = 21.6654 dB.

The noisy Barbara image with high-level Gaussian noise; variance = 0.1 & mean = 0 is shown in Fig. 4.6 (a). The corresponding reconstructed Barbara image using circular wavelet de-noising scheme is shown in Fig. 4.6 (b) with Correlation = 0.9140 and PSNR = 17.9.

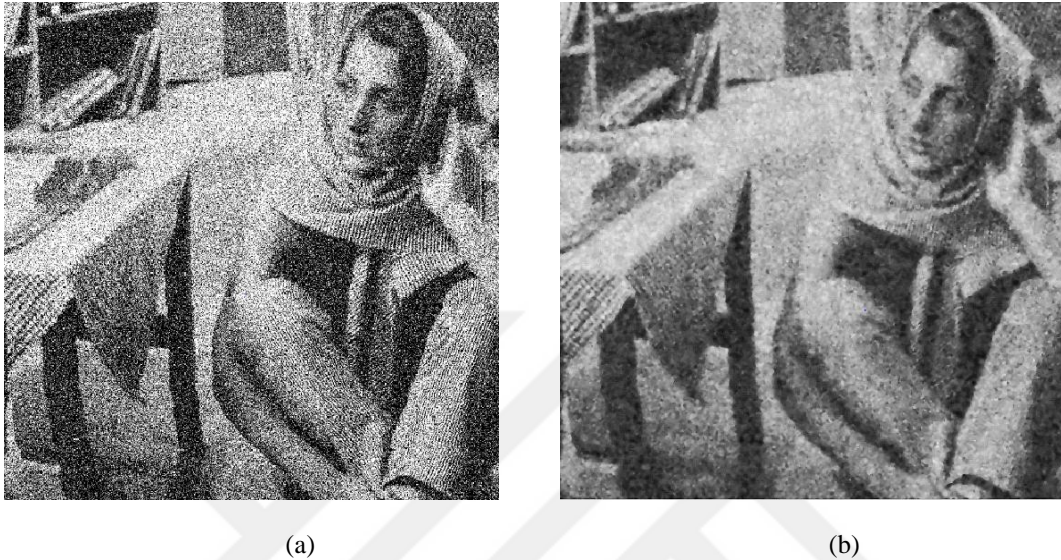


Fig. 4.6 (a) Noisy Barbara image with high-level Gaussian noise; variance = 0.1 & mean = 0, (b) The corresponding reconstructed Barbara image using circular wavelet de-noising scheme; Correlation = 0.9140 and PSNR = 17.9298 dB.

The noisy Lena image with low-level Gaussian noise; variance = 0.001 & mean = 0 is shown in Fig. 4.7 (a). The corresponding reconstructed Lena image using circular wavelet de-noising scheme is shown in Fig. 4.7 (b) with Correlation = 0.9921 and PSNR = 31.6530 dB.



Fig. 4.7 (a) Noisy Lena image with low-level Gaussian noise; variance = 0.001 & mean = 0, (b) The corresponding reconstructed Lena image using circular wavelet de-noising scheme; Correlation = 0.9921 and PSNR = 31.6530 dB.

The noisy Lena image with mid-level Gaussian noise; variance = 0.01 & mean = 0 is shown in Fig. 4.8 (a). The corresponding reconstructed Lena image using circular wavelet de-noising scheme is shown in Fig. 4.8 (b) with Correlation = 0.9833 and PSNR = 28.3812 dB.

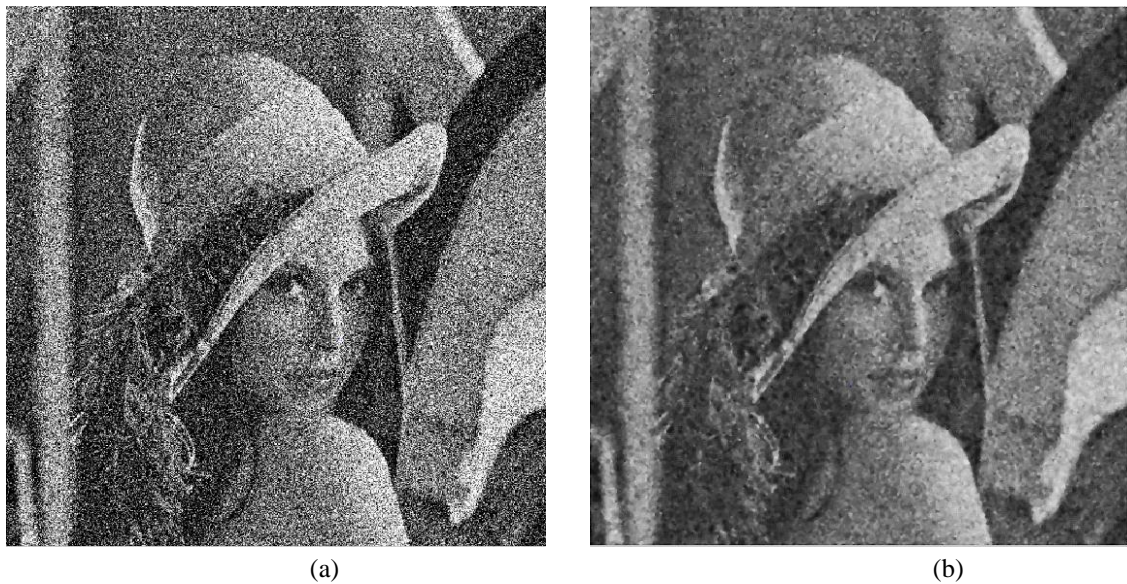


Fig. 4.8 (a) Noisy Lena image with mid-level Gaussian noise; variance = 0.01 & mean = 0, (b) The corresponding reconstructed Lena image using circular wavelet de-noising scheme; Correlation = 0.9833 and PSNR = 28.3812 dB.

The noisy Lena image with high-level Gaussian noise; variance = 0.1 & mean = 0 is shown in Fig. 4.9 (a). The corresponding reconstructed Lena image using circular wavelet de-noising scheme is shown in Fig. 4.9 (b) with Correlation = 0.9074 and PSNR = 20.4518 dB.



Fig . 4. 9 (a) . Noisy Lena image with high-level Gaussian noise; variance = 0.1 & mean = 0, (b) The corresponding reconstructed Lena image using circular wavelet de-noising scheme; Correlation = 0.9074 and PSNR = 20.4518 dB.

The noisy Boat image with low-level Gaussian noise; variance = 0.001 & mean = 0 is shown in Fig. 4.10 (a). The corresponding reconstructed Boat image using circular wavelet de-noising scheme is shown in Fig. 4.10 (b) with Correlation = 0.9822 and PSNR = 29.2190 dB.



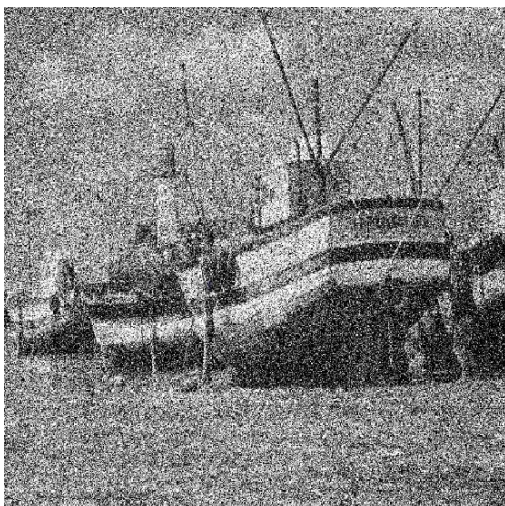
(a)



(b)

Fig. 4.10 (a) Noisy Boat image with low-level Gaussian noise; variance = 0.001 & mean = 0, (b) The corresponding reconstructed Boat image using circular wavelet de-noising scheme; Correlation = 0.9822 and PSNR = 29.2190 dB.

The noisy Boat image with mid-level Gaussian noise; variance = 0.01 & mean = 0 is shown in Fig. 4.11 (a). The corresponding reconstructed Boat image using circular wavelet de-noising scheme is shown in Fig. 4.11 (b) with Correlation = 0.9701 and PSNR = 27.0098 dB.



(a)



(b)

Fig. 4.11 (a) Noisy Boat image with mid-level Gaussian noise; variance = 0.01 & mean = 0, (b) The corresponding reconstructed Boat image using circular wavelet de-noising scheme; Correlation = 0.9701 and PSNR = 27.0098 dB.

The noisy Boat image with high-level Gaussian noise; variance = 0.1 & mean = 0 is shown in Fig. 4.12 (a). The corresponding reconstructed Boat image is shown in Fig. 4.12 (b) with Correlation = 0.9004 and PSNR = 21.8580 dB.



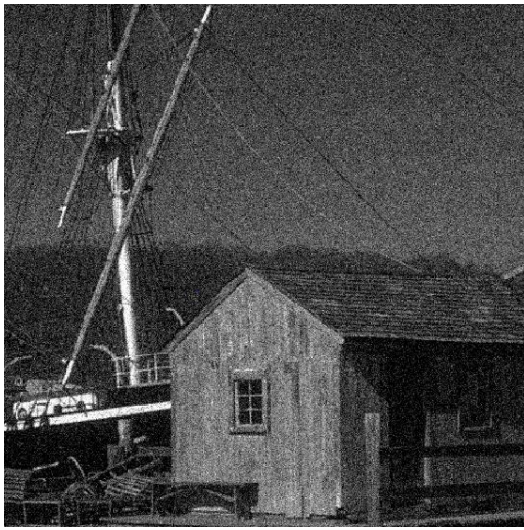
(a)



(b)

Fig. 4.12 (a) Noisy Boat image with high-level Gaussian noise; variance = 0.1 & mean = 0, (b) The corresponding reconstructed Boat image using circular wavelet de-noising scheme; Correlation = 0.9004 and PSNR = 21.8580 dB.

The noisy House image with low-level Gaussian noise; variance = 0.001 & mean = 0 is shown in Fig. 4.13 (a). The corresponding reconstructed House image using circular wavelet de-noising scheme is shown in Fig. 4.13 (b) with Correlation = 0.9752 and PSNR = 29.4985 dB.



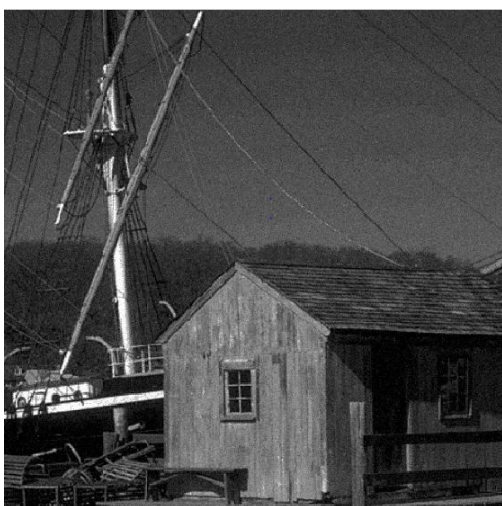
(a)



(b)

Fig. 4.13 (a) Noisy House image with low-level Gaussian noise; variance = 0.001 & mean = 0, (b) The corresponding reconstructed House image using circular wavelet de-noising scheme; Correlation = 0.9752 and PSNR = 29.4985 dB.

The noisy House image with mid-level Gaussian noise; variance = 0.01 & mean = 0 is shown in Fig. 4.14 (a). The corresponding reconstructed House image using circular wavelet de-noising scheme is shown in Fig. 4.14 (b) with Correlation = 0.9557 and PSNR = 26.9520 dB.



(a)



(b)

Fig. 4.14 (a) Noisy House image with mid-level Gaussian noise; variance = 0.01 & mean = 0, (b) The corresponding reconstructed House image using circular wavelet de-noising scheme; Correlation = 0.9557 and PSNR = 26.9520 dB.

The noisy House image with high-level Gaussian noise; variance = 0.1 & mean = 0 is shown in Fig. 4.15 (a). The corresponding reconstructed House image using circular wavelet de-noising scheme is shown in Fig. 4.15 (b) with Correlation = 0.8557 and PSNR = 21.1640 dB.

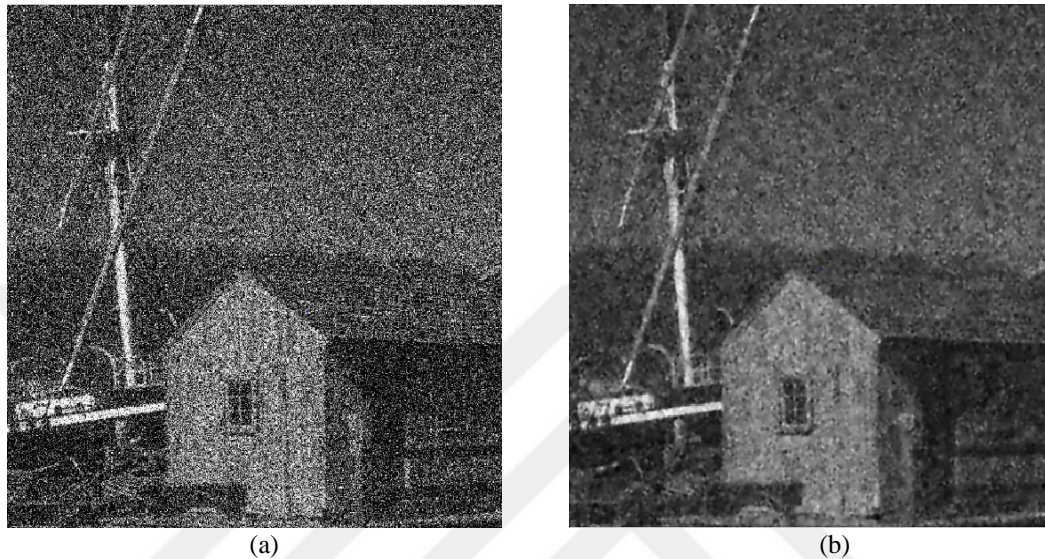


Fig. 4.15 (a) Noisy House image with high-level Gaussian noise; variance = 0.1 & mean = 0, (b) The corresponding reconstructed House image using circular wavelet de-noising scheme; Correlation = 0.8557 and PSNR = 21.1640 dB.

4.1.2. Circular wavelet results for images with salt and pepper noise

In this sub-section, the performance of the proposed circular wavelet de-noising scheme is evaluated via the same pre-mentioned five testing noisy images. Three levels of salt and pepper noise densities are used in the evaluation. These levels of noise densities are low-level noise density of 0.001, mid-level noise density of 0.01 and high-level noise density of 0.1. The noisy Camera man image with a low-level noise density of 0.001 (salt and pepper noise) is shown in Fig. 4.16 (a). The corresponding reconstructed Camera man image using circular wavelet de-noising scheme is shown in Fig. 4.16 (b) with Correlation = 0.9820 and PSNR = 27.3281 dB.



(a)



(b)

Fig. 4.16 (a) Noisy Camera man image with a low-level noise density of 0.001 (salt and pepper noise), (b) The corresponding reconstructed Camera man image using circular wavelet de-noising scheme; Correlation = 0.9820 and PSNR = 27.3281 dB.

The noisy Camera man image with a mid-level noise density of 0.01 (salt and pepper noise) is shown in Fig. 4.17 (a). The corresponding reconstructed Camera man image using circular wavelet de-noising scheme is shown in Fig. 4.17 (b) with Correlation = 0.9810 and PSNR = 26.4481 dB.



(a)



(b)

Fig. 4.17 (a) Noisy Camera man image with a mid-level noise density of 0.01 (salt and pepper noise), (b) The corresponding reconstructed Camera man image using circular wavelet de-noising scheme; Correlation = 0.9810 and PSNR = 26.4481 dB.

The noisy Camera man image with a high-level noise density of 0.1 (salt and pepper noise) is shown in Fig. 4.18 (a). The corresponding reconstructed Camera man image using circular wavelet de-noising scheme is shown in Fig. 4.18 (b) with Correlation = 0.9617 and PSNR = 23.4019 dB.

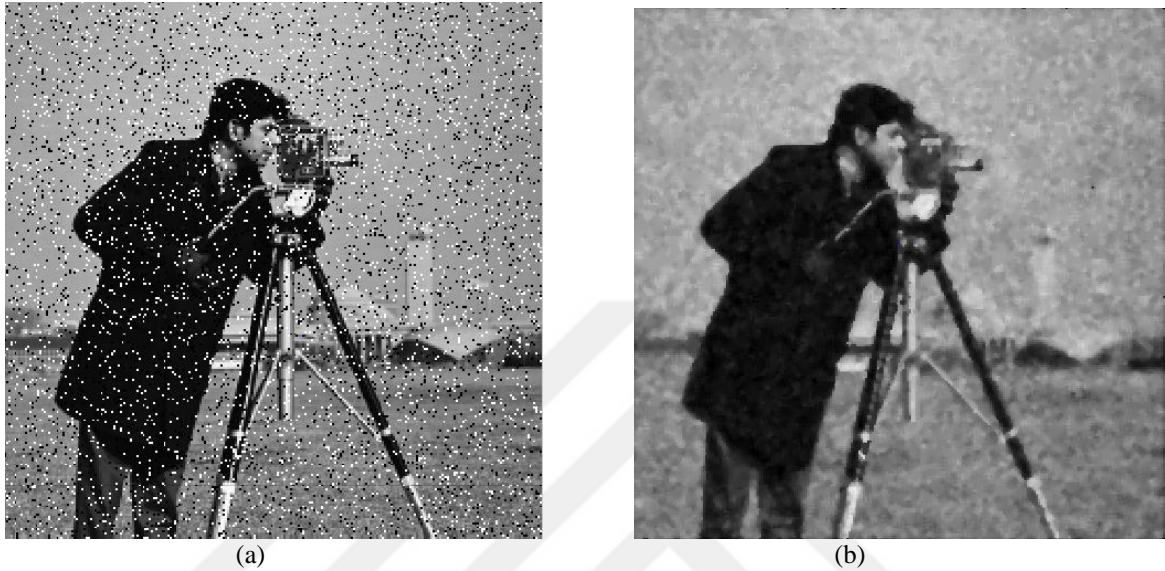


Fig. 4.18 (a) Noisy Camera man image with a high-level noise density of 0.1 (salt and pepper noise), (b) The corresponding reconstructed Camera man image using circular wavelet de-noising scheme; Correlation = 0.9617 and PSNR = 23.4019 dB.

The noisy Barbara image with a low-level noise density of 0.001 (salt and pepper noise) is shown in Fig. 4.19 (a). The corresponding reconstructed Barbara image using circular wavelet de-noising scheme is shown in Fig. 4.19 (b) with Correlation = 0.9635 and PSNR = 22.4161 dB.



(a)



(b)

Fig. 4.19 (a) Noisy Barbara image with a low-level noise density of 0.001 (salt and pepper noise), (b) The corresponding reconstructed Barbara image using circular wavelet de-noising scheme; Correlation = 0.9635 and PSNR = 22.4161 dB.

The noisy Barbara image with a mid-level noise density of 0.01 (salt and pepper noise) is shown in Fig. 4.20 (a). The corresponding reconstructed Barbara image using circular wavelet de-noising scheme is shown in Fig. 4.20 (b) with Correlation = 0.9624 and PSNR = 22.2895 dB.



(a)



(b)

Fig. 4.20 (a) Noisy Barbara image with a mid-level noise density of 0.01 (salt and pepper noise), (b) The corresponding reconstructed Barbara image using circular wavelet de-noising scheme; Correlation = 0.9624 and PSNR = 22.2895 dB.

The noisy Barbara image with a high-level noise density of 0.1 (salt and pepper noise) is shown in Fig. 4.21 (a). The corresponding reconstructed Barbara image using circular wavelet de-noising scheme is shown in Fig. 4.21 (b) with Correlation = 0.9478 and PSNR = 20.8331 dB.

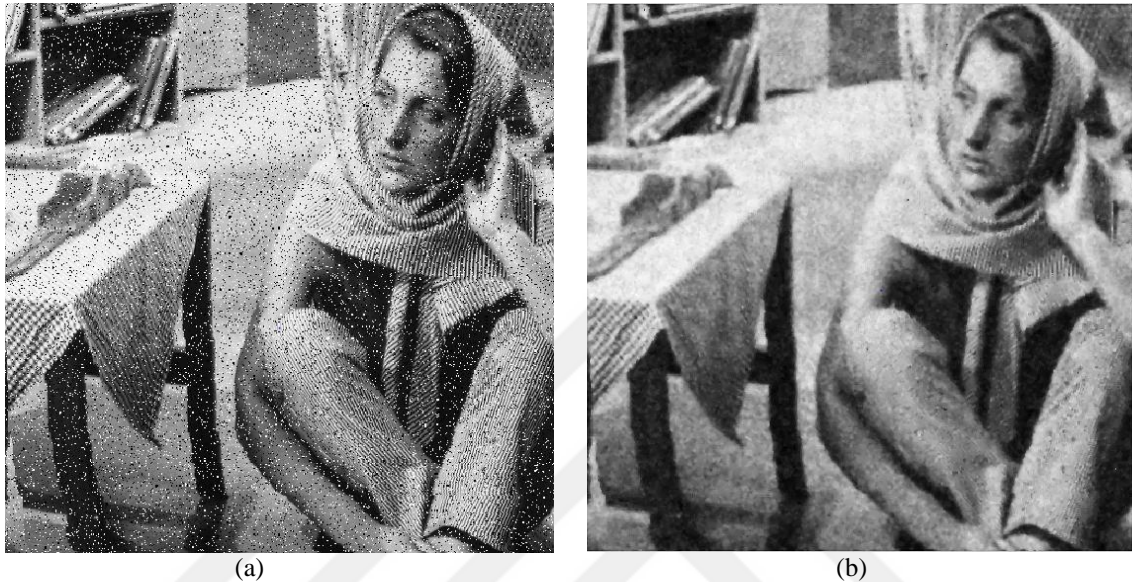


Fig. 4.21 (a) Noisy Barbara image with a high-level noise density of 0.1 (salt and pepper noise), (b) The corresponding reconstructed Barbara image using circular wavelet de-noising scheme; Correlation = 0.9478 and PSNR = 20.8331 dB.

The noisy Lena image with a low-level noise density of 0.001 (salt and pepper noise) is shown in Fig. 4.22 (a). The corresponding reconstructed Lena image using circular wavelet de-noising scheme is shown in Fig. 4.22 (b) with Correlation = 0.9932 and PSNR = 32.2770 dB.



Fig. 4.22 (a) Noisy Lena image with a low-level noise density of 0.001 (salt and pepper noise), (b) The corresponding reconstructed Lena image using circular wavelet de-noising scheme; Correlation = 0.9932 and PSNR = 32.2770 dB.

The noisy Lena image with a mid-level noise density of 0.01 (salt and pepper noise) is shown in Fig. 4.23 (a). The corresponding reconstructed Lena image using circular wavelet de-noising scheme is shown in Fig. 4.23 (b) with Correlation = 0.9916 and PSNR = 31.3539 dB.

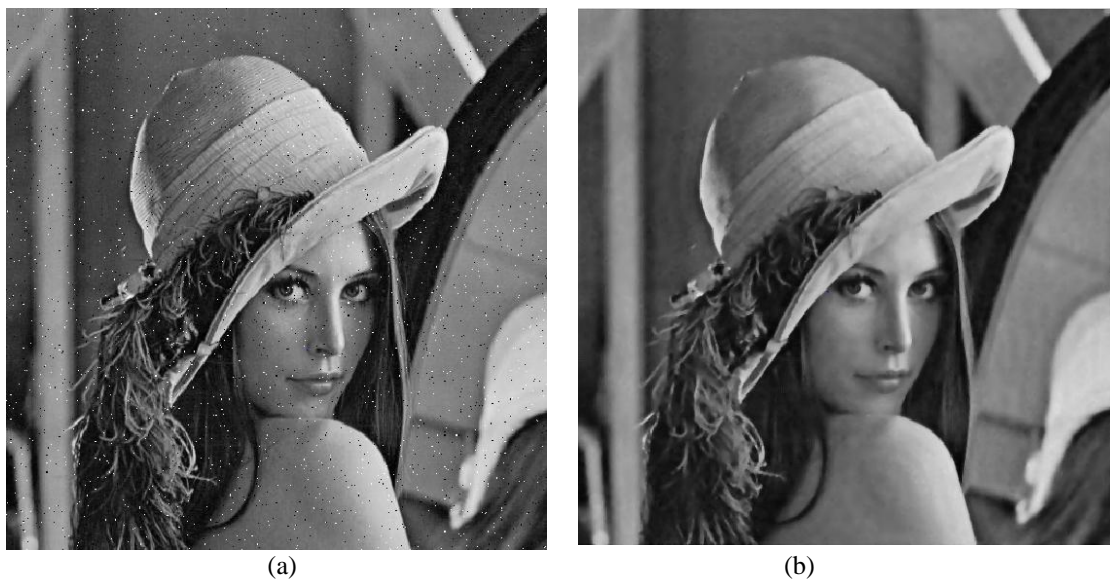


Fig. 4.23 (a) Noisy Lena image with a mid-level noise density of 0.01 (salt and pepper noise), (b) The corresponding reconstructed Lena image using circular wavelet de-noising scheme; Correlation = 0.9916 and PSNR = 31.3539 dB.

The noisy Lena image with a high-level noise density of 0.1 (salt and pepper noise) is shown in Fig. 4.24 (a). The corresponding reconstructed Lena image using circular wavelet de-noising scheme is shown in Fig. 4.24 (b) with Correlation = 0.9733 and PSNR = 26.4267 dB.



Fig. 4.24 (a) Noisy Lena image with a high-level noise density of 0.1 (salt and pepper noise), (b) The corresponding reconstructed Lena image using circular wavelet de-noising scheme; Correlation = 0.9733 and PSNR = 26.4267 dB.

The noisy Boat image with a low-level noise density of 0.001 (salt and pepper noise) is shown in Fig. 4.25 (a). The corresponding reconstructed Boat image using circular wavelet de-noising scheme is shown in Fig. 4.25 (b) with Correlation = 0.9835 and PSNR = 29.5365 dB.



(a)



(b)

Fig. 4.25 (a) Noisy Boat image with a low-level noise density of 0.001 (salt and pepper noise), (b) The corresponding reconstructed Boat image using circular wavelet de-noising scheme; Correlation = 0.9835 and PSNR = 29.5365 dB.

The noisy Boat image with a mid-level noise density of 0.01 (salt and pepper noise) is shown in Fig. 4.26 (a). The corresponding reconstructed Boat image using circular wavelet de-noising scheme is shown in Fig. 4.26 (b) with Correlation = 0.9812 and PSNR = 28.9975 dB.



(a)



(b)

Fig. 4.26 (a) Noisy Boat image with a mid-level noise density of 0.01 (salt and pepper noise), (b) The corresponding reconstructed Boat image using circular wavelet de-noising scheme; Correlation = 0.9812 and PSNR = 28.9975 dB.

The noisy Boat image with a high-level noise density of 0.1 (salt and pepper noise) is shown in Fig. 4.27 (a). The corresponding reconstructed Boat image using circular wavelet de-noising scheme is shown in Fig. 4.27 (b) with Correlation = 0.9531 and PSNR = 25.1218 dB.

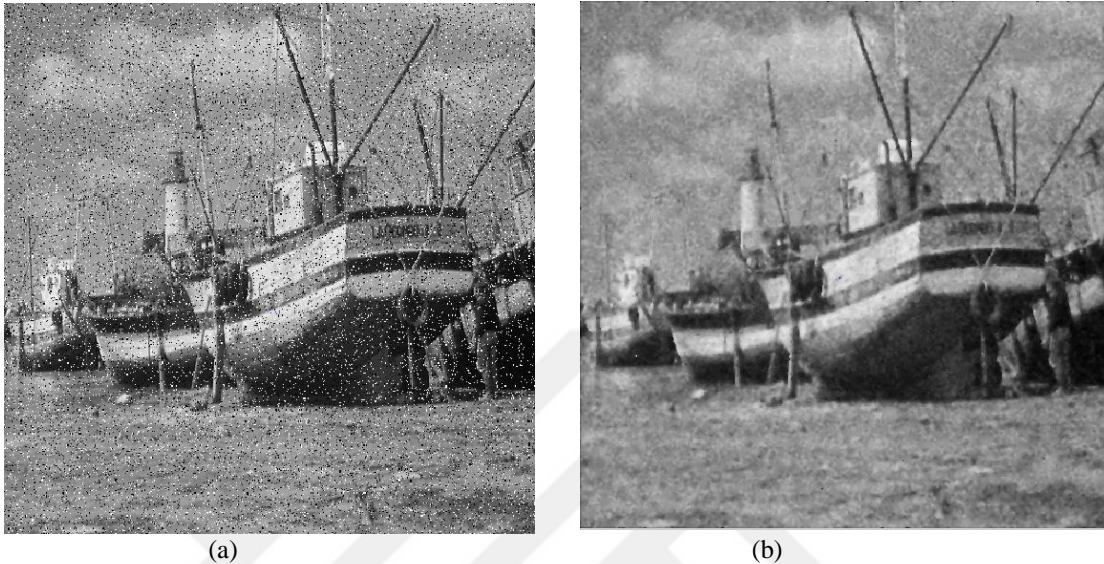


Fig. 4.27 (a) Noisy Boat image with a high-level noise density of 0.1 (salt and pepper noise), (b) The corresponding reconstructed Boat image using circular wavelet de-noising scheme; Correlation = 0.9531 and PSNR = 25.1218 dB.

The noisy House image with a low-level noise density of 0.001 (salt and pepper noise) is shown in Fig. 4.28 (a). The corresponding reconstructed House image using circular wavelet de-noising scheme is shown in Fig. 4.28 (b) with Correlation = 0.9774 and PSNR = 29.9080 dB.



Fig. 4.28 (a) Noisy House image with a low-level noise density of 0.001 (salt and pepper noise), (b) The corresponding reconstructed House image using circular wavelet de-noising scheme; Correlation = 0.9774 and PSNR = 29.9080 dB.

The noisy House image with a mid-level noise density of 0.01 (salt and pepper noise) is shown in Fig. 4.29 (a). The corresponding reconstructed House image using circular wavelet de-noising scheme is shown in Fig. 4.29 (b) with Correlation = 0.9728 and PSNR = 29.1222 dB.

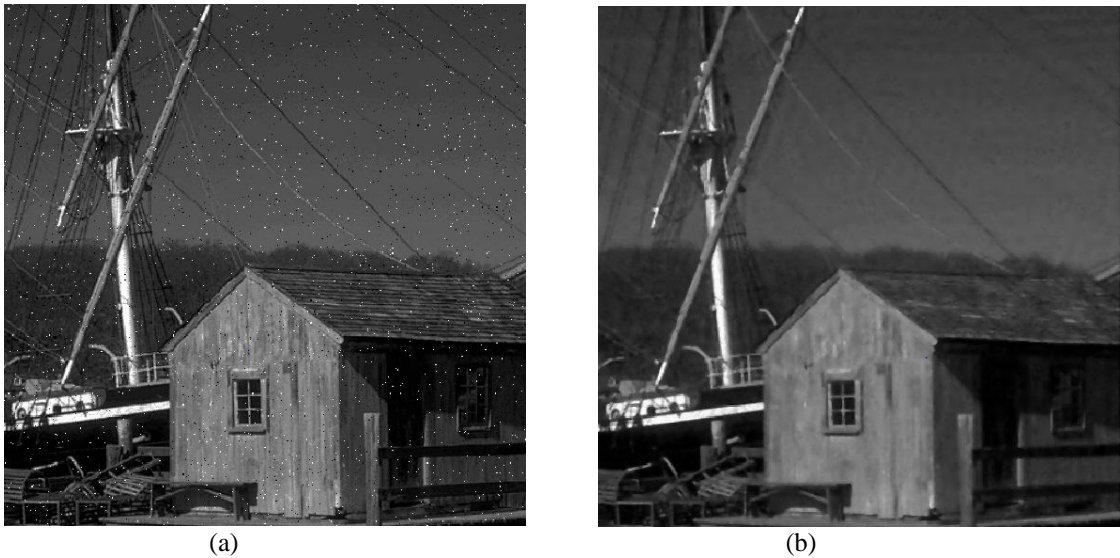


Fig. 4.29 (a) Noisy House image with a mid-level noise density of 0.01 (salt and pepper noise), (b) The corresponding reconstructed House image using circular wavelet de-noising scheme; Correlation = 0.9728 and PSNR = 29.1222 dB.

The noisy House image with a high-level noise density of 0.1 (salt and pepper noise) is shown in Fig. 4.30 (a). The corresponding reconstructed House image using circular wavelet de-noising scheme is shown in Fig. 4.30 (b) with Correlation = 0.9369 and PSNR = 25.5504 dB.

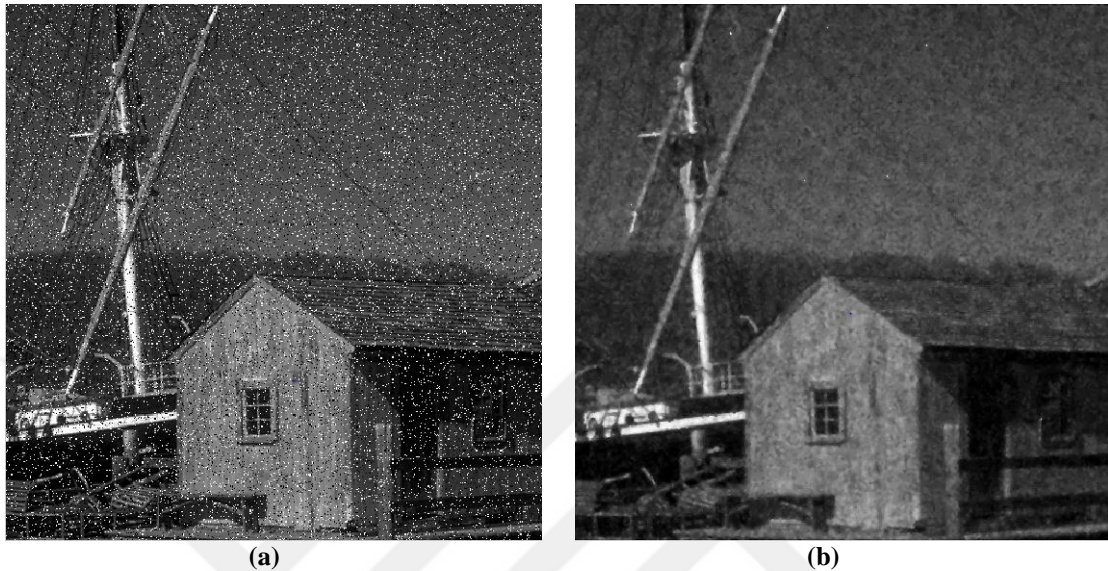


Fig. 4.30 (a) Noisy House image with a high-level noise density of 0.1 (salt and pepper noise), (b) The corresponding reconstructed House image using circular wavelet de-noising scheme; Correlation = 0.9369 and PSNR = 25.5504 dB.

4.2. Results of Conventional wavelet de-noising by thresholding

The conventional wavelet de-noising by thresholding is tested in this section on the same pre-mentioned testing five noisy images with three different levels of Gaussian noise and then with Salt and pepper noise. We will start in the next sub-section with the results obtained by examination of three different levels of Gaussian noise.

4.2.1. Conventional wavelet Results for images with Gaussian noise

In this sub-section, the performance of the conventional wavelet de-noising by thresholding is evaluated by testing the same pre-mentioned five noisy test images. The same three pre-defined levels of Gaussian noise are used in that evaluation. The noisy Camera man image with low-level Gaussian noise; variance = 0.001 & mean = 0 is shown in Fig. 4.31 (a). The corresponding reconstructed Camera man image using conventional

wavelet de-noising by thresholding is shown in Fig. 4.31 (b) with Correlation = 0.9891 and PSNR = 28.8598 dB.

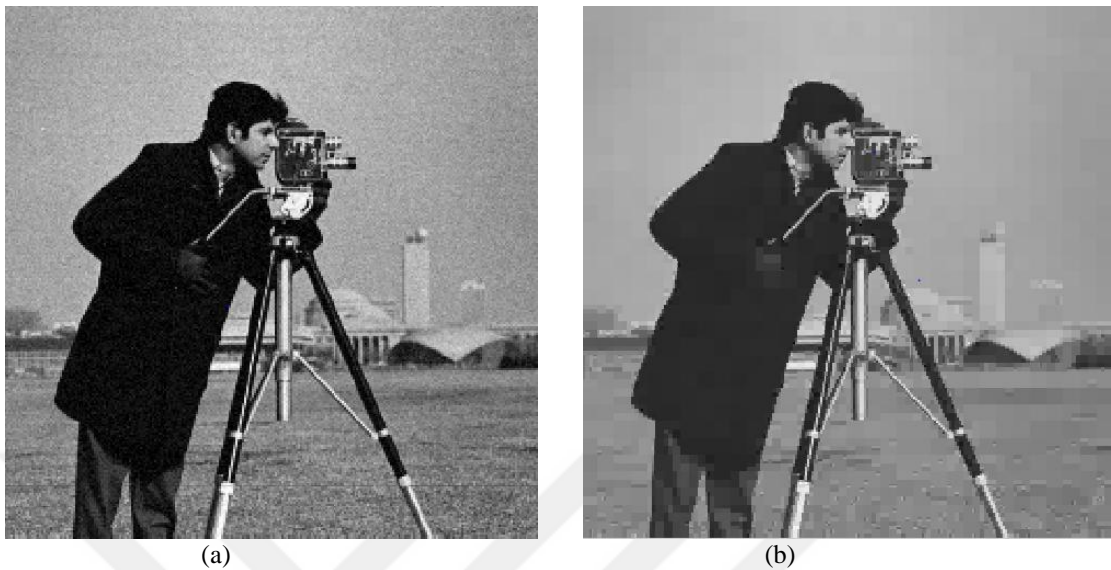


Fig. 4.31 (a) Noisy Camera man image with low-level Gaussian noise; variance = 0.001 & mean = 0, (b) The corresponding reconstructed Camera man image using conventional wavelet de-noising by thresholding; Correlation = 0.9891 and PSNR = 28.8598 dB.

The noisy Camera man image with mid-level Gaussian noise; variance = 0.01 & mean = 0 is shown in Fig. 4.32 (a). The corresponding reconstructed Camera man image using conventional wavelet de-noising by thresholding is shown in Fig. 4.32 (b) with Correlation = 0.9643 and PSNR = 23.6263 dB.

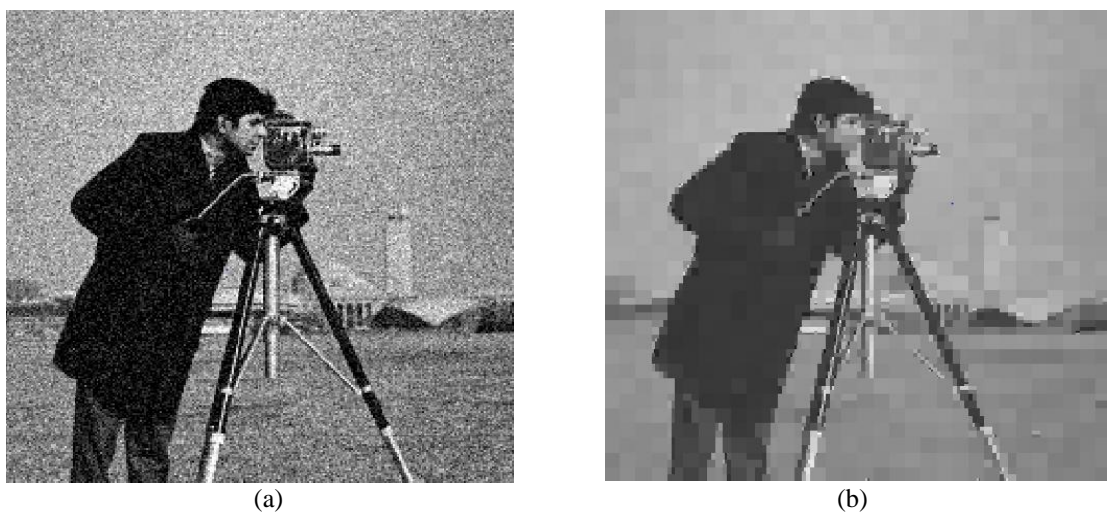


Fig. 4.32 (a) Noisy Camera man image with mid-level Gaussian noise; variance = 0.01 & mean = 0, (b) The corresponding reconstructed Camera man image using conventional wavelet de-noising by thresholding; Correlation = 0.9643 and PSNR = 23.6263 dB.

The noisy Camera man image with high-level Gaussian noise; variance = 0.1 & mean = 0 is shown in Fig. 4.33 (a). The corresponding reconstructed Camera man image using conventional wavelet de-noising by thresholding is shown in Fig. 4.33 (b) with Correlation = 0.8997 and PSNR = 18.9302 dB.

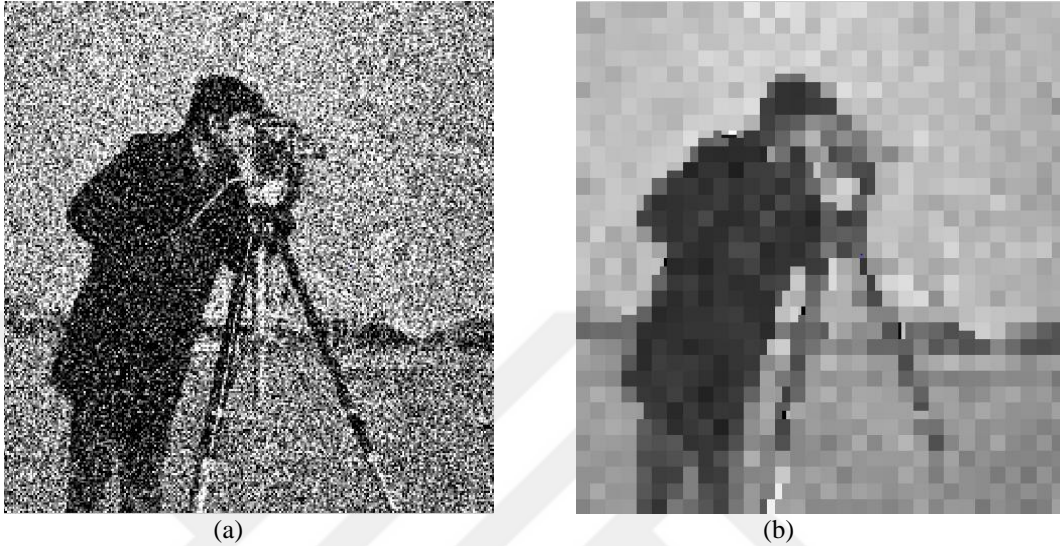


Fig. 4.33 (a) Noisy Camera man image with high-level Gaussian noise; variance = 0.1 & mean = 0, (b) The corresponding reconstructed Camera man image using conventional wavelet de-noising by thresholding; Correlation = 0.8997 and PSNR = 18.9302 dB.

The noisy Barbara image with low-level Gaussian noise; variance = 0.001 & mean = 0 is shown in Fig. 4.34 (a). The corresponding reconstructed Barbara image using conventional wavelet de-noising by thresholding is shown in Fig. 4.34 (b) with Correlation = 0.9789 and PSNR = 24.7756 dB.

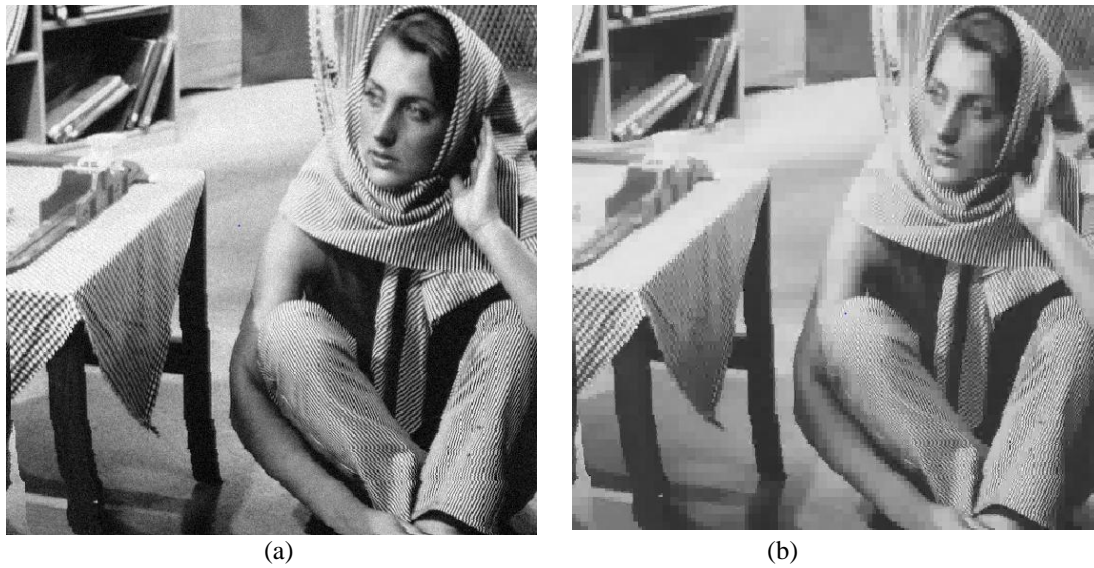


Fig. 4.34 (a) Noisy Barbara image with low-level Gaussian noise; variance = 0.001 & mean = 0, (b) The corresponding reconstructed Barbara image using conventional wavelet de-noising by thresholding; Correlation = 0.9789 and PSNR = 24.7756 dB.

The noisy Barbara image with mid-level Gaussian noise; variance = 0.01 & mean = 0 is shown in Fig. 4.35 (a). The corresponding reconstructed Barbara image using conventional wavelet de-noising by thresholding is shown in Fig. 4.35 (b) with Correlation = 0.9462 and PSNR = 20.4983 dB.

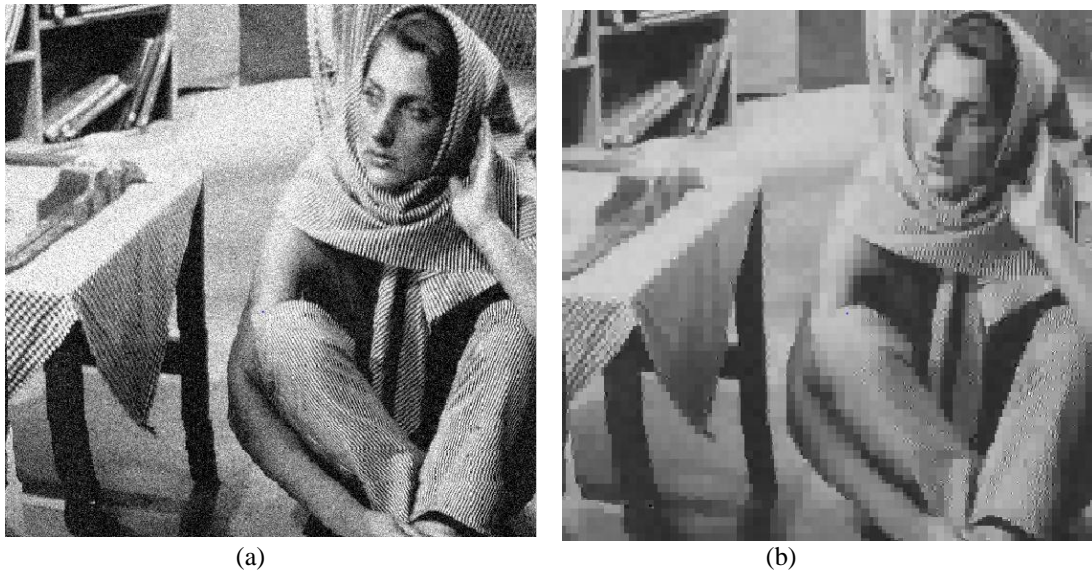


Fig. 4.35 (a) Noisy Barbara image with mid-level Gaussian noise; variance = 0.01 & mean = 0, (b) The corresponding reconstructed Barbara image using conventional wavelet de-noising by thresholding; Correlation = 0.9462 and PSNR = 20.4983 dB.

The noisy Barbara image with high-level Gaussian noise; variance = 0.1 & mean = 0 is shown in Fig. 4.36 (a). The corresponding reconstructed Barbara image using conventional wavelet de-noising by thresholding is shown in Fig. 4.36 (b) with Correlation = 0.9037 and PSNR = 17.8011 dB.

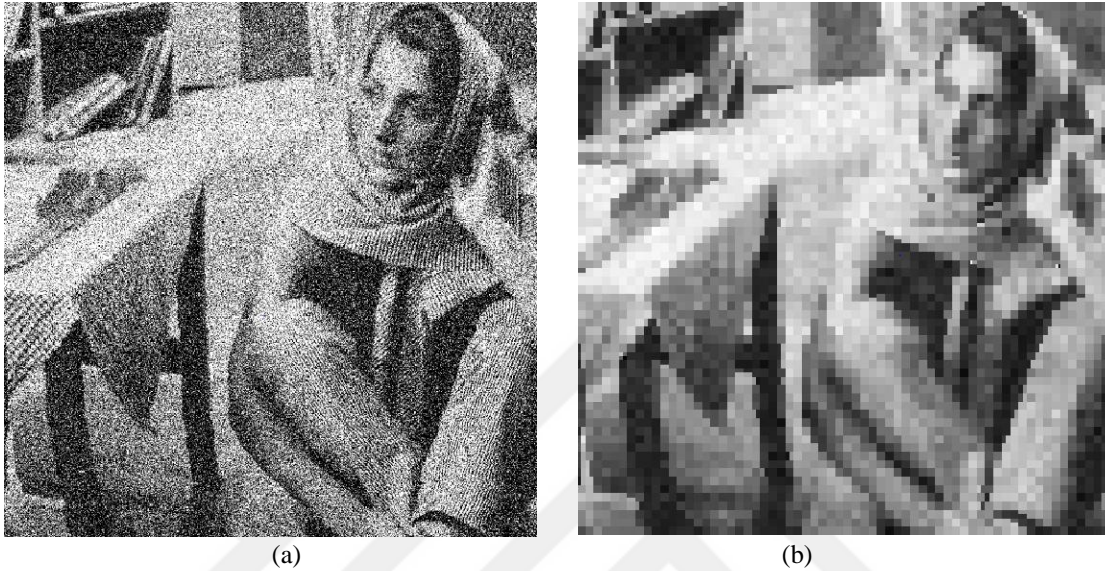


Fig. 4.36 (a) Noisy Barbara image with high-level Gaussian noise; variance = 0.1 & mean = 0, (b) The corresponding reconstructed Barbara image using conventional wavelet de-noising by thresholding; Correlation = 0.9037 and PSNR = 17.8011 dB.

The noisy Lena image with low-level Gaussian noise; variance = 0.001 & mean = 0 is shown in Fig. 4.37 (a). The corresponding reconstructed Lena image using conventional wavelet de-noising by thresholding is shown in Fig. 4.37 (b) with Correlation = 0.9869 and PSNR = 29.5199 dB.

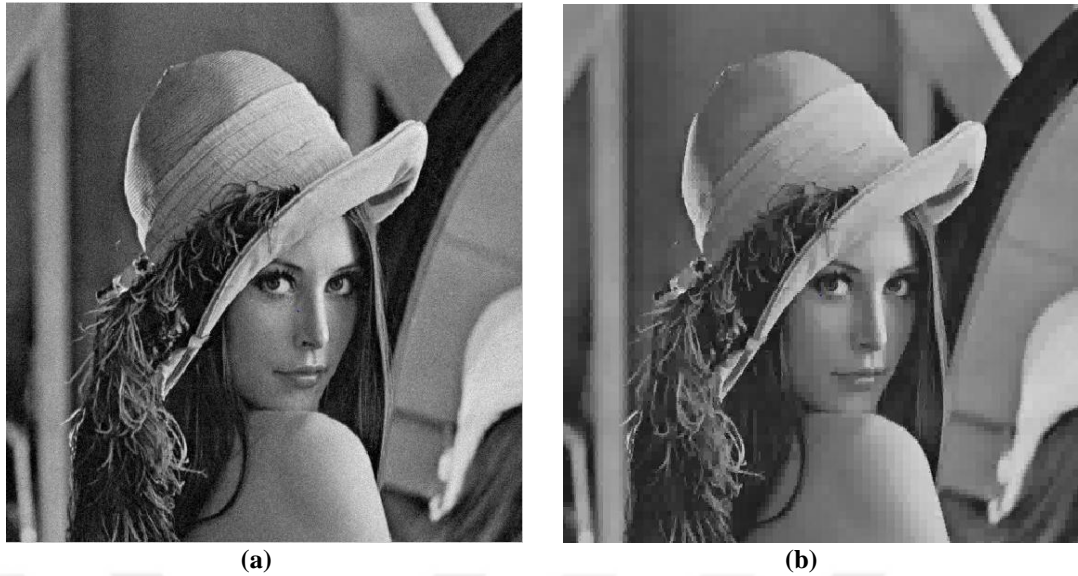


Fig. 4.37 (a) Noisy Lena image with low-level Gaussian noise; variance = 0.001 & mean = 0, (b) The corresponding reconstructed Lena image using conventional wavelet de-noising by thresholding; Correlation = 0.9869 and PSNR = 29.5199 dB.

The noisy Lena image with mid-level Gaussian noise; variance = 0.01 & mean = 0 is shown in Fig. 4.38 (a). The corresponding reconstructed Lena image using conventional wavelet de-noising by thresholding is shown in Fig. 4.38 (b) with Correlation = 0.9636 and PSNR = 25.1233 dB.



Fig. 4.38 (a) Noisy Lena image with mid-level Gaussian noise; variance = 0.01 & mean = 0, (b) The corresponding reconstructed Lena image using conventional wavelet de-noising by thresholding; Correlation = 0.9636 and PSNR = 25.1233 dB.

The noisy Lena image with high-level Gaussian noise; variance = 0.1 & mean = 0 is shown in Fig. 4.39 (a). The corresponding reconstructed Lena image using conventional wavelet de-noising by thresholding is shown in Fig. 4.39 (b) with Correlation = 0.9187 and PSNR = 21.0460 dB.

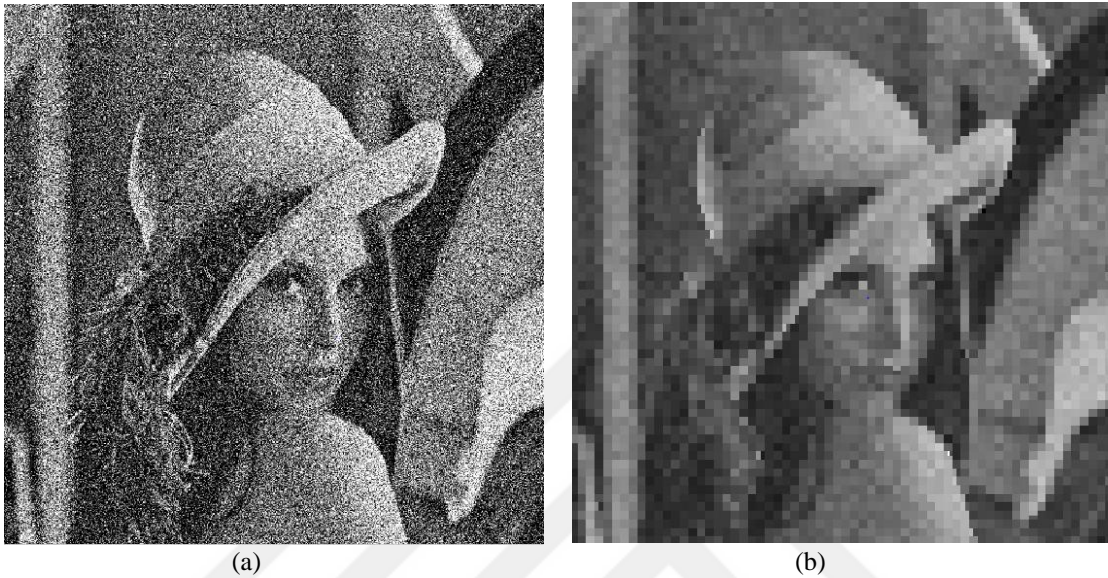


Fig. 4.39 (a) Noisy Lena image with high-level Gaussian noise; variance = 0.1 & mean = 0, (b) The corresponding reconstructed Lena image using conventional wavelet de-noising by thresholding; Correlation = 0.9187 and PSNR = 21.0460 dB.

The noisy Boat image with low-level Gaussian noise; variance = 0.001 & mean = 0 is shown in Fig. 4.40 (a). The corresponding reconstructed Boat image using conventional wavelet de-noising by thresholding is shown in Fig. 4.40 (b) with Correlation = 0.9771 and PSNR = 28.1933 dB.



(a)



(b)

Fig. 4.40 (a) Noisy Boat image with low-level Gaussian noise; variance = 0.001 & mean = 0, (b) The corresponding reconstructed Boat image using conventional wavelet de-noising by thresholding; Correlation = 0.9771 and PSNR = 28.1933 dB.

The noisy Boat image with mid-level Gaussian noise; variance = 0.01 & mean = 0 is shown in Fig. 4.41 (a). The corresponding reconstructed Boat image using conventional wavelet de-noising by thresholding is shown in Fig. 4.41 (b) with Correlation = 0.9419 and PSNR = 24.2219 dB.



(a)



(b)

Fig. 4.41 (a) Noisy Boat image with mid-level Gaussian noise; variance = 0.01 & mean = 0, (b) The corresponding reconstructed Boat image using conventional wavelet de-noising by thresholding; Correlation = 0.9419 and PSNR = 24.2219 dB.

The noisy Boat image with high-level Gaussian noise; variance = 0.1 & mean = 0 is shown in Fig. 4.42 (a). The corresponding reconstructed Boat image using conventional

wavelet de-noising by thresholding is shown in Fig. 4.42 (b) with Correlation = 0.8791 and PSNR = 20.9727 dB.

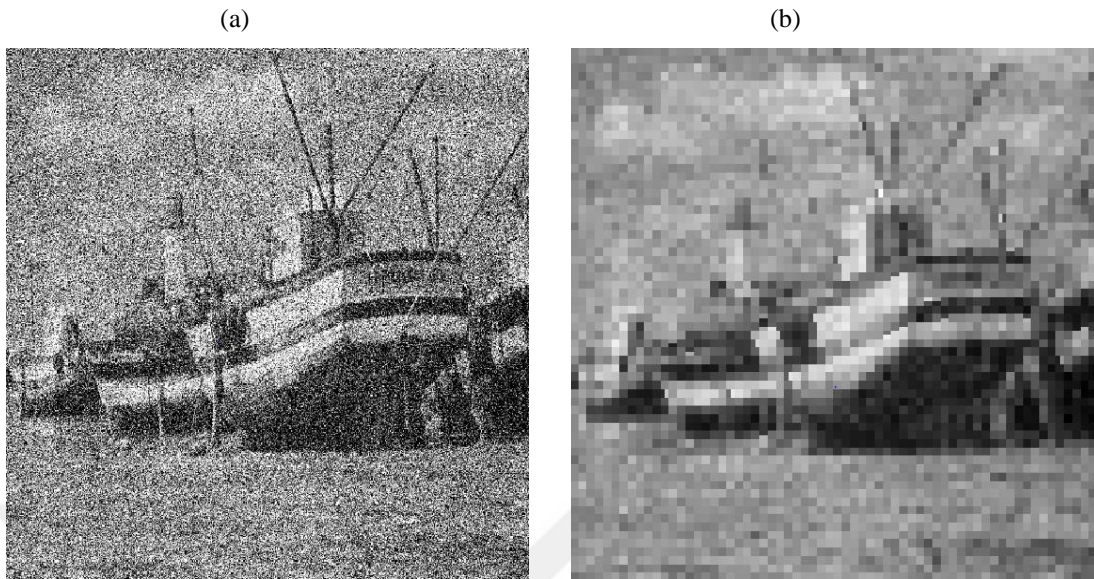


Fig. 4.42 (a) Noisy Boat image with high-level Gaussian noise; variance = 0.1 & mean = 0, (b) The corresponding reconstructed Boat image using conventional wavelet de-noising by thresholding; Correlation = 0.8791 and PSNR = 20.9727 dB.

The noisy House image with low-level Gaussian noise; variance = 0.001 & mean = 0 is shown in Fig. 4.43 (a). The corresponding reconstructed House image using conventional wavelet de-noising by thresholding is shown in Fig. 4.43 (b) with Correlation = 0.9715 and PSNR = 28.9806 dB.

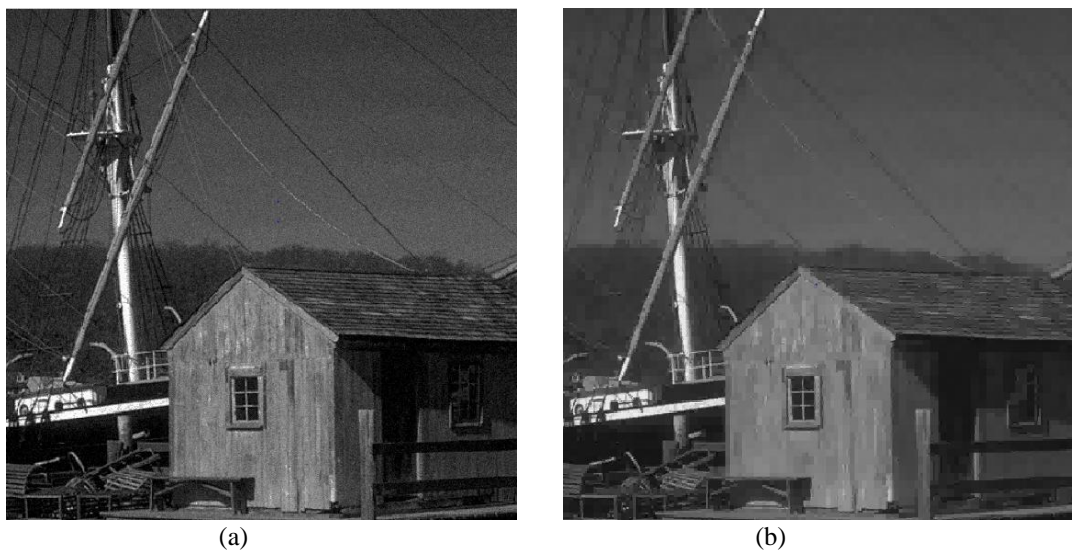


Fig. 4.43 (a) Noisy House image with low-level Gaussian noise; variance = 0.001 & mean = 0, (b) The corresponding reconstructed House image using conventional wavelet de-noising by thresholding; Correlation = 0.9715 and PSNR = 28.9806 dB.

The noisy House image with mid-level Gaussian noise; variance = 0.01 & mean = 0 is shown in Fig. 4.44 (a). The corresponding reconstructed House image using conventional wavelet de-noising by thresholding is shown in Fig. 4.44 (b) with Correlation = 0.9272 and PSNR = 24.9794 dB.

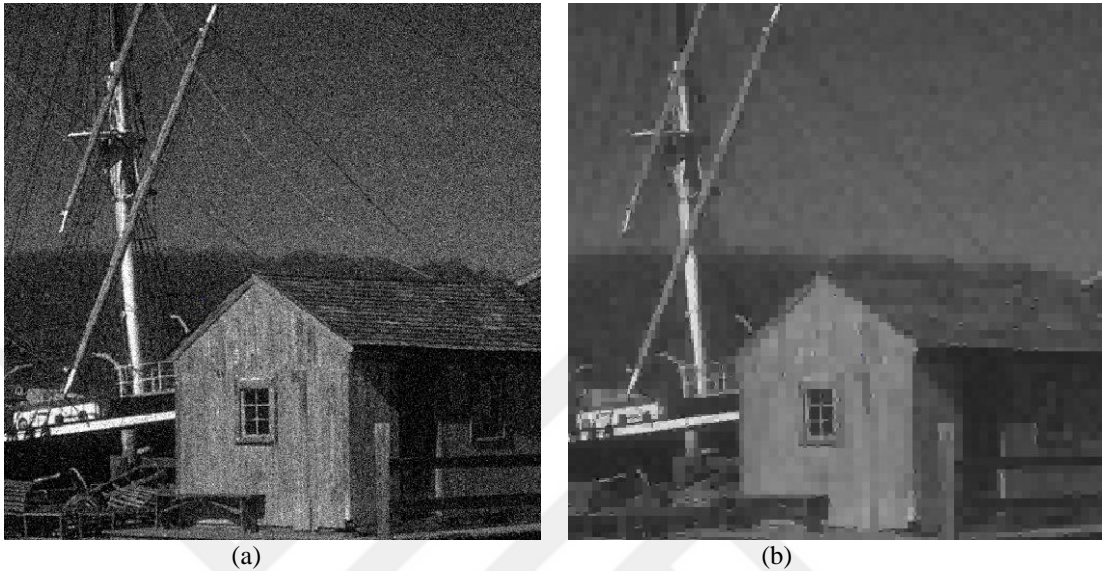


Fig. 4.44 (a) Noisy House image with mid-level Gaussian noise; variance = 0.01 & mean = 0, (b) The corresponding reconstructed House image using conventional wavelet de-noising by thresholding; Correlation = 0.9272 and PSNR = 24.9794 dB.

The noisy House image with high-level Gaussian noise; variance = 0.1 & mean = 0 is shown in Fig. 4.45 (a). The corresponding reconstructed House image using conventional wavelet de-noising by thresholding is shown in Fig. 4.45 (b) with Correlation = 0.8417 and PSNR = 20.7389 dB.

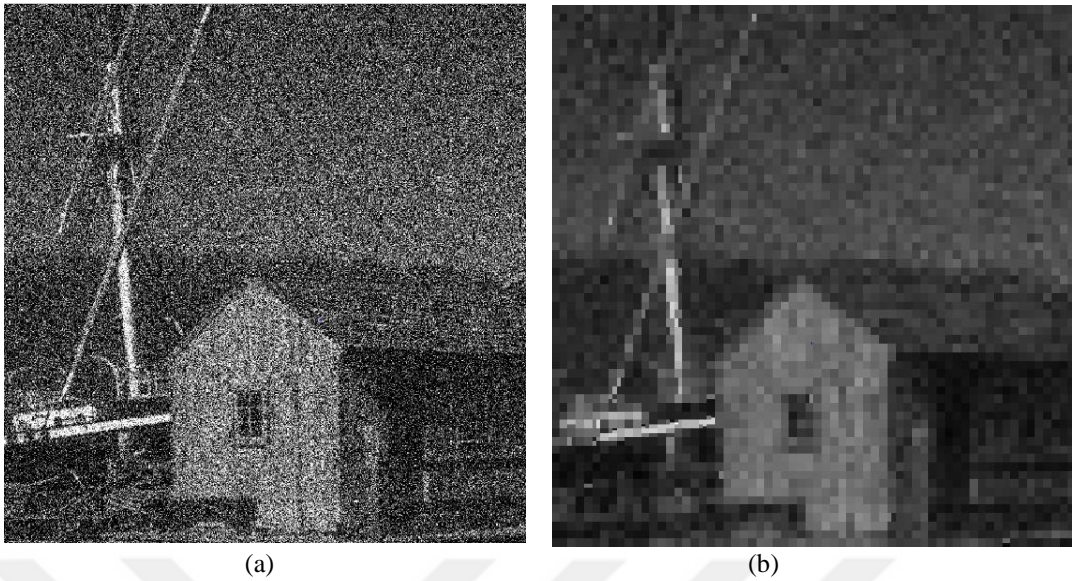


Fig. 4.45 (a) Noisy House image with high-level Gaussian noise; variance = 0.1 & mean = 0, (b) The corresponding reconstructed House image using conventional wavelet de-noising by thresholding; Correlation = 0.8417 and PSNR = 20.7389 dB.

4.2.2. Conventional wavelet Results for images with salt and pepper Noise

It has been noted that conventional wavelet de-noising by thresholding cannot handle the salt and pepper noise and almost has no effect on the image. So, the tests by the conventional wavelet de-noising on noisy images (with salt and pepper noise) are cancelled.

4.3. A Comparative Study

A summarized comparison between different obtained results is given in this section. The comparison highlights different Correlation factor values and PSNR values achieved throughout all tests on the pre mentioned five images (Camera man, Barbara, Lena, Boat and House). These values have been resulted from applying conventional wavelet de-noising method and from the application of the proposed circular wavelet de-noising scheme. Tables 4.1 and 4.2 summarize such results for the five test images.

Table 4.1. Resulting Correlation factors and PSNR values for different noisy images from the applications of both conventional wavelet de-noising method and the proposed circular wavelet de-noising scheme; (with Gaussian noise).

Gaussian Noise Level		0.001		0.01		0.1	
Method	Image	Corr.	PSNR (dB)	Corr.	PSNR (dB)	Corr.	PSNR (dB)
Conventional Wavelet De-Noising	Camera man	0.9891	28.8598	0.9643	23.6263	0.8997	18.9302
	Barbara	0.9789	24.7756	0.9462	20.4983	0.9037	17.8011
	Lena	0.9869	29.5199	0.9636	25.1233	0.9187	21.0460
	Boat	0.9771	28.1933	0.9419	24.2219	0.8791	20.9727
	House	0.9715	28.9806	0.9272	24.9794	0.8417	20.7389
Proposed Circular Wavelet De-Noising Scheme	Camera man	0.9808	26.4181	0.9738	24.9231	0.9245	20.0761
	Barbara	0.9644	22.5153	0.9571	21.6654	0.9140	17.9298
	Lena	0.9921	31.6530	0.9833	28.3812	0.9074	20.4518
	Boat	0.9822	29.2190	0.9701	27.0098	0.9004	21.8580
	House	0.9752	29.4985	0.9701	27.0098	0.9004	21.8580

From Table 4.1, it can be seen that the proposed circular wavelet de-noising scheme in many cases give results in the same order of those for the conventional wavelet de-noising method for low-level Gaussian noise (variance= 0.001). While better performance can be obtained from the proposed circular scheme as the Gaussian noise level is increased which means the proposed scheme is more suitable exactly for medium-level noise values (variance= 0.01) and generally for high-level noise values (variance= 0.1).

Table 4.2. Resulting Correlation factors and PSNR values for different noisy images from the applications of both conventional wavelet de-noising method and the proposed circular wavelet de-noising scheme; (with salt and pepper noise)

salt and pepper Noise Level		0.001		0.01		0.1	
Method	Image	Corr.	PSNR (dB)	Corr.	PSNR (dB)	Corr.	PSNR (dB)
Conventional Wavelet De-Noising	Camera man	----	----	----	----	----	----
	Barbara	----	----	----	----	----	----
	Lena	----	----	----	----	----	----
	Boat	----	----	----	----	----	----
	House	----	----	----	----	----	----
Proposed Circular Wavelet De-Noising Scheme	Camera man	0.9820	27.3281	0.9810	26.4481	0.9617	23.4019
	Barbara	0.9635	22.4161	0.9624	22.2895	0.9478	20.8331
	Lena	0.9932	32.2770	0.9916	31.3539	0.9733	26.4267
	Boat	0.9835	29.5365	0.9812	28.9975	0.9531	25.1218
	House	0.9774	29.9080	0.9728	29.1222	0.9369	25.5504

From Table 4.2, it can be easily seen that the conventional wavelet de-noising method cannot perform well with salt and pepper noise and almost has no effect on noisy image. Thus, for conventional wavelet de-noising method, the results are omitted.

5. CONCLUSIONS AND FUTURE WORK

5.1. Conclusions

A new image de-noising scheme based on a two-dimensional circular-support wavelet transform (2-D CSWT) has been proposed, constructed and tested. This 2-D CSWT is a geometrical image transform constructed using 2-D circular spectral split schemes which have been realized efficiently using frequency-masking for the resulting filter bank branches. The performance of the proposed system has been examined by calculating metrics; such as correlation factors and PSNR values of the resulting reconstructed de-noised images.

A comparative study has been accomplished between the proposed circular wavelet de-noising scheme and the conventional wavelet de-noising method. The proposed de-noising scheme and in many cases have shown some results in the same order of those for the conventional wavelet de-noising method for low-level Gaussian noise (variance= 0.001). A better performance has been obtained from the proposed scheme as the Gaussian noise level is increased which means the proposed scheme is more suitable exactly for medium-level noise values (variance= 0.01) and generally for high-level noise values (variance= 0.1).

It has been noticed that the conventional wavelet de-noising method cannot perform well with salt and pepper noise and almost has no effect on noisy image, whereas the proposed scheme shows a good de-noising performance.

5.2. Future Works

The future work can be directed to one of the followings:

- 1) The scheme can further analyzed to have more decomposition levels more than 3 for better de-noising performance.
- 2) The frequency masking filters can be realized as approximate hardware filters for hardware implementations of the whole scheme.
- 3) A homomorphic circular wavelet-based de-speckling technique can be used as an extension to the proposed circular wavelet de-noising scheme to reduce speckles in Synthetic Aperture Radar (SAR) and ultrasound images. The homomorphic environment converts multiplicative speckle model into an additive noise one.



REFERENCES

- Abdul-Jabbar, J. M., 2009, An analytical design procedure for Bireciprocal Lattice Wave Digital Filters with approximate linear phase, *Alrafidain Engineering Journal, Collage of Engineering, University of Mosul, Mosul, Iraq*, 17 (6), 42-52.
- Abdul-Jabbar, J. M. and Abdulkader, Z. N., 2010, Design and Realization of Circular Contourlet Transform, *Al-Rafidain Engineering Journal*, Vol. 18, No. 4, , pp. 28 - 42.
- Abdul-Jabbar, J. M., 2011, A Simple Analytic Design Procedure for Lattice Wave Digital Filters with Approximate Linear Phase, *Basrah Journal for Engineering Science*.
- Abdul-Jabbar, J. M. and Abdulkader, Z. N., 2012, Iris recognition using 2-D elliptical-support wavelet filter bank, *Image Processing Theory, Tools and Applications (IPTA), 2012 3rd International Conference on*, 359-363.
- Abdul-Jabbar, J. M., Abede, Z. T. and Dawood, A. A., 2013, A Multiplier-less Implementation of Two-Dimensional Circular-Support Wavelet Transform on FPGA, *Iraqi Journal for Electrical & Electronic Engineering*, 9 (1).
- Akansu, A. N. and Haddad, R. A., 2001, Multiresolution signal decomposition: transforms, subbands, and wavelets, Academic Press, p.
- Buades, A., Coll, B. and Morel, J.-M., 2005, A review of image denoising algorithms, with a new one, *Multiscale Modeling & Simulation*, 4 (2), 490-530.
- Chen, J., Benesty, J., Huang, Y. and Doclo, S., 2006, New insights into the noise reduction Wiener filter, *IEEE Transactions on audio, speech, and language processing*, 14 (4), 1218-1234.
- Chui, C. K., 1992, Wavelets: a tutorial in theory and applications, *Wavelet Analysis and its Applications, San Diego, CA: Academic Press,| c1992, edited by Chui, Charles K*.

Chui, C. K., 2016, An introduction to wavelets, Elsevier, p.

Combes, J.-M., Grossmann, A. and Tchamitchian, P., 2012, Wavelets: Time-Frequency Methods and Phase Space Proceedings of the International Conference, Marseille, France, December 14–18, 1987, Springer Science & Business Media, p.

Daubechies, I., 1988, Orthonormal bases of compactly supported wavelets, *Communications on Pure and Applied Mathematics*, 41 (7), 909-996.

Demir, B. and Erturk, S., 2007, Wavelet Denoising Before Support Vector Classification of Hyperspectral Images, *Signal Processing and Communications Applications, 2007. SIU 2007. IEEE 15th*, 1-4.

Ergen, B. and Baykara, M., 2011, ANALYSIS OF DENOISING WITH WAVELET AND WAVELET PACKAGE DECOMPOSITION METHODS, *Engineering Sciences*, 6 (2), 518-526.

Ergen, B., 2012, Signal and image denoising using wavelet transform, In: *Advances in Wavelet Theory and Their Applications in Engineering, Physics and Technology*, Eds: InTech, p.

Fliege, N. J., 1994, Multirate digital signal processing, John Wiley New York, p.

Johansson, H. and Wanhammar, L., 1996, Design of birectiprocal linear-phase lattice wave digital filters, Univ., p.

M. İkiz, M. Akin, B.Kurt and Acar, H., 2007, Recognition The Speaker Identity By Means Of Wavelet Analysis And Neural Network, *Dogu Anadolu Bolgesi Arastirmalari*.

Mallat, S. G., 1989, A theory for multiresolution signal decomposition: the wavelet representation, *IEEE transactions on pattern analysis and machine intelligence*, 11 (7), 674-693.

Mastriani, M., 2015, Quantum Boolean image denoising, *Quantum Information Processing*, 14 (5), 1647-1673.

Shinde, B., Mhaske, D. and Dani, A., 2012, Study of noise detection and noise removal techniques in medical images, *International Journal of Image, Graphics and Signal Processing*, 4 (2), 51.

Shukla, K. K. and Tiwari, A. K., 2013, Efficient algorithms for discrete wavelet transform: with applications to denoising and fuzzy inference systems, Springer Science & Business Media, p.

Singh, M. K., 2010, Denoising of natural images using the wavelet transform, San Jose State University, p.

Srivastava, A. and Maheshwari, S., 2015, Signal Denoising and Multiresolution Analysis by Discrete Wavelet Transform *Innovative Trends in Applied Physical, Chemical, Mathematical Sciences and Emerging Energy Technology for Sustainable Development*.

Strang, G. and Nguyen, T., 1996, Wavelets and filter banks, SIAM, p.

Üstündağ, M., Engin, A., Gökbulut, M. and Fikret, A., 2014, Dalgacık paket dönüşümü ve genetik algoritma kullanarak zayıf radar sinyallerinin gürültüden arındırılması, *Gazi Üniversitesi Mühendislik-Mimarlık Fakültesi Dergisi*, 29 (2).

Vaidyanathan, P., 1993, Multirate Systems and Filter Banks. Prentice Hall. Englewood Cliffs.

Vatansever, F., Uysal, F. and Uzun, A., 2002, Ayrik Dalgacık Dönüşümü ile Gürültü Süzme, ELECO.

Verma, R. and Ali, D. J., 2013, A comparative study of various types of image noise and efficient noise removal techniques, *International journal of advanced research in computer science and software engineering*, 3 (10).

Xiong, C., Tian, J. and Liu, J., 2007, Efficient architectures for two-dimensional discrete wavelet transform using lifting scheme, *IEEE transactions on image processing*, 16 (3), 607-614.



ÖZGEÇMİŞ

KİŞİSEL BİLGİLER

Adı Soyadı : ADIL AYDIKI
Uyruğu : IRAK
Doğum Yeri ve Tarihi : MUSUL 1987
Telefon : 05347664416
Faks :
e-mail : adil.shingary86@hotmail.com

EĞİTİM

Derece	Adı, İlçe, İl	Bitirme Yılı
Lise	: Alrisala Lisesi	2007
Üniversite	: AL-Hdbaa Üniversitesi	2011

İŞ DENEYİMLERİ

Yıl	Kurum	Görevi
-----	-------	--------

UZMANLIK ALANI Bilişim ve Teknoloji Mühendisliği

YABANCI DİLLER İngilizce, Arapça

BELİRTMEK İSTEĞİNİZ DİĞER ÖZELLİKLER

YAYINLAR

Adil A. Y. AYDIKI, Omar YASEEN ISMAEL and Fatih BAŞÇİFTÇİ, (2018), “Image De-noising using 2-D Circular-Support Wavelet Transform ”, American Scientific Research Journal for Engineering, Technology, and Sciences (ASRJETS), ISSN (Print) 2313-4410, ISSN (Online) 2313-4402, Vol.42, No 1, pp: 1-13.